The Mechanism of Proton Transport in Imidazolium-Based and Hydronium-Based Protic Ionic Liquid Systems

by

Aurelia A. Moses

Submitted in Partial Fulfillment of the Requirements

for the Degree of

Master of Science

in the

Chemistry

Program

YOUNGSTOWN STATE UNIVERSITY

August, 2022

The Mechanism of Proton Transport in Imidazolium-Based and Hydronium-Based Protic Ionic Liquid Systems

Aurelia A. Moses

I hereby release this thesis to the public. I understand that this thesis will be made available from the OhioLINK ETD Center and the Maag Library Circulation Desk for public access. I also authorize the University or other individuals to make copies of this thesis as needed for scholarly research.

Signature:

Aurelia A. Moses, Student Date

Approvals:

Dr. Christopher Arntsen, Thesis Advisor Date

Dr. Brian Leskiw, Committee Member Date

Dr. Clovis Linkous, Committee Member Date

Dr. Salvatore A. Sanders, Dean of Graduate Studies Date

Acknowledgements

I would like to thank the Department of Chemical and Biological Sciences at Youngstown State University for their support throughout the past two years of my career. Both the faculty and staff in the department have gone above and beyond to help me succeed.

I would also like to thank the other students in my year, Brandi, Van and Vincent, for their support as both esteemed colleagues and as friends. I feel grateful to have had them in my cohort and I wish them all the best as they move forward in their careers.

The help of Jonah Weisman, an undergraduate of the Arntsen lab, was invaluable. I'm grateful for Jonah's assistance in running simulations and analysis that would have otherwise been overwhelming to do on my own.

I would like to thank the Ohio Supercomputer Center for the use of their resources throughout the past two years.

I would like to thank my advisor, Dr. Chris Arntsen, for his mentorship, encouragement, and advice over the past two years. Thanks to Dr. Arntsen, I have learned a brand-new set of skills that I can carry into the rest of my career. Projects didn't always yield the results we expected and the thrill of diving into the unknown in the Arntsen lab is unrivaled. Dr. Arntsen's excitement over the research has consistently reminded me why I love my field of study. Thanks to Dr. Arntsen, my future is open to many wonderful opportunities and I have gained the confidence to step into the next phase of my career.

Finally, I would like to thank my parents and my sister for their encouragement over the past two years. Their support was integral to my motivation and they have

consistently challenged me to understand my research better by asking me questions and genuinely trying to understand my work, and in doing so, causing me to understand my project well enough to explain it simply.

Abstract

The mechanism of proton transport was studied computationally using *ab initio* molecular dynamics (AIMD) in three protic ionic liquid (PIL) systems to determine how charge diffusion was impacted by various factors. Such ionic liquids can be used to increase the efficiency of proton-conducting layers in hydrogen fuel cells so the fuel cells can operate at higher temperatures without expending as much labor and cost to do so. The first system used n-ethylimidazolium (C_2HIm^+) as a cation and determined how the addition of a solvent changed the rate of diffusion as well as changing the anion, using both the anion form of bis(trifluoromethanesulfonyl)imide ($TFSI^-$) and acetate ion. The second set of simulations were similar to the first, but used a simpler [HIm^+][$TFSI^-$] and determined the effect of temperature on PILs with added solvent over an 80 K range. Finally, a third set of simulations was run to determine the mechanism of proton transport in a solvate ionic liquid (SIL) system with 18-crown-6-ether•H_3O^+ used as the cation and running simulations containing both $TFSI^-$ and acetate as the anion. The research outlined in this thesis shows that these systems can be reliably studied computationally with AIMD and allows insight for a greater understanding of these systems.

Table of Contents

List of Chapters

List of Figures

List of Tables

List of Equations

1. Introduction

1.1 Ionic Liquids

Ionic liquids (IL) are disordered systems composed of charged particles which have low volatility, high ionic conductivity, and the potential to solvate added species. Characteristics vary based on the subset of ILs as different types can be used for different purposes. Unlike molten salts, most ILs have low melting temperatures, and room-temperature ILs (RTILs) are naturally liquids below 373 K. RTILs can be used as green alternatives in organic catalysis and synthesis since they are unique in consisting of ionic organic compounds and allow for organic reactions to run at much lower temperatures.[1] ILs have been researched for over 100 years, but they are so versatile that much research is still needed in the area. Combinations of different cations and anions must be characterized and the uses of ILs are being explored because ILs can be tailored to fit a variety of functions depending on the application. One of the most well-categorized IL pairs are 1,3-ethylmethylimidazolium ($EMIM^+$) and bis(trifluoromethanesulfonyl)imide

($TFSI^-$), shown in Fig. 1. These ion pairs create a thermodynamically stable RTIL and can be considered a prototypical IL.

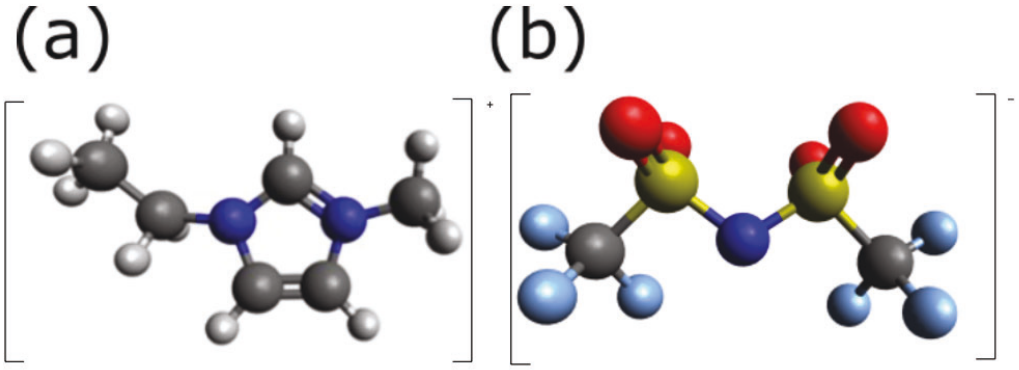

Figure 1: A common IL featuring EMIM (a) and TFSI (b).

Research surrounding ILs is versatile due to their many possible functions as ILs are easily customizable by using different cation-anion pairs depending on the function the IL must serve. For instance, ILs can be used in porous materials like metal-organic frameworks (MOFs) where ILs fill the pores of the polymers and facilitate charge conduction or separation and purification. Amine ILs have been used in conjunction with MOFs to facilitate air filtration because the amine IL can covalently bind to CO_2 and successfully capture it.[2] The specification of amine ILs for CO_2 capture is ideal due to the low energy of regeneration for CO_2 capture. In such systems, water is often added to the pure IL to facilitate CO_2 capture. The addition of a solvent such as water is another common practice to customize ILs further to fulfill specific purposes.

Various neutral solvents can be added to ILs to form IL mixtures, depending on their compatibility with the ion pairs and the desired function the IL must serve. Besides air purification, water is a commonly added solvent for aid in metal extraction[3] or proton transfer.[4] Water's small size and polar properties make it an ideal solvent, but it has been

found to be incompatible with some ILs.[4] Therefore, organic solvents can be selected based on factors such as size or solubility, once again depending on the IL ion pair and the necessary function of the IL.

1.2 Protic Ionic Liquids

A subset of ILs known as protic ionic liquids (PILs) are a target area of research in green energy since PILs contain acidic protons on the cation which can potentially transport across the system by hopping from one species to the next. Depending on the ionicity of the IL mixture, acidic protons can transfer via the cation-anion pair or via an added solvent and the path of proton transfer will be determined by the relative $\mathrm{p}K_\mathrm{a}$ of the species. If the protonated form of any species in the mixture has a $\mathrm{p}K_\mathrm{a}$ too low to accept a proton, the proton will not transfer to that species. An ideal difference in $\mathrm{p}K_\mathrm{a}$ between the ion pairs is 10 in order to create a pure IL without neutral species,[5] and as such, the anion in many ILs are unable to accept a proton due to the high acidity of the conjugate acid. However, when the purity and ionicity of the IL is not a consideration in its function, the IL may have neutral species. Regardless, the presence of transferrable protons creates a high potential for proton conductivity in PILs, making them ideal charge conductors which have potential applications to fuel cells.

Proton transport can occur via two possible mechanisms: the Grotthuss mechanism or the vehicular transport mechanism. Systems that use the vehicular mechanism transport a charge via a parent ion. A charged particle diffuses through the system and as it diffuses, the charge diffuses with it. The pure IL mixture of $EMIM^+$ and $TFSI^-$ conduct negative and positive charges in this manner. $EMIM^+$ carries a charge which

diffuses through the system as the ion itself diffuses. Lithium batteries also undergo vehicular transport where Li^+ diffuses through the system, carrying the charge.[3] Vehicular transport is the only mechanism of charge transport in systems where a charge is unable to disconnect from the parent ion in an energetically-favorable manner but is also a common mechanism for PILs, despite the transferrable proton. The ability of a proton to transfer is dependent primarily on the $\mathrm{p}K_\mathrm{a}$ of the various species in the PIL so it is therefore not always able to transfer the charge to another species and the charge will diffuse via vehicular transport as the excess proton remains attached to the parent ion.

An alternative mechanism of charge transport, proposed over 200 years ago,[6] can apply to some PILs if the excess proton is able to transfer to other species in the IL mixture. The Grotthuss mechanism transports a charge on excess protons which "hop" from one species to the next, as seen schematically in Fig. 2, allowing for rapid charge diffusion with little displacement of nuclear coordinates. Hydronium is known to have a high diffusion coefficient of $9.31 \times 10^{-9}\ \mathrm{m}^2/\mathrm{s}$, which is significantly higher than the diffusion of similarly sized ions that undergo vehicular transport (see Table 1). Ions capable of undergoing Grotthuss hopping have a more rapid diffusion than ions traveling via vehicular transport.[7]

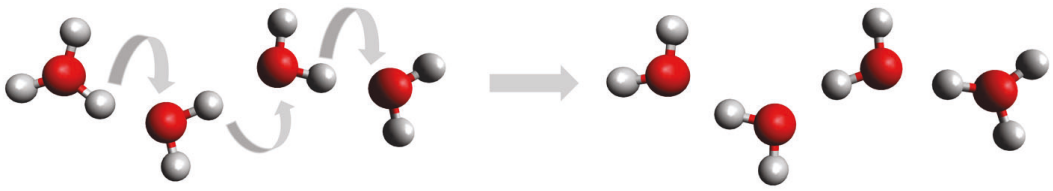

Figure 2: Transfer of an excess proton in water via the Grotthuss mechanism.

Table 1: The rate of diffusion of various ions.[7]

Ion	D [10^9 m^2/s]
H_3O^+	9.31
Li^+	1.03
Na^+	1.33
K^+	1.96

PILs must meet various conditions to undergo the Grotthuss mechanism.[8] A PIL must contain species that are able to accept a proton. Otherwise, the excess proton will be transported on the parent ion via vehicular transport. Although C_2HIm^+, pictured in Fig. 3, possesses an excess proton with the ability to hydrogen bond and hop, the proton will not transfer unless there is a species that can accept it. Whether or not the proton transports via the Grotthuss mechanism is dependent on the anion used and any solvents added to the IL.

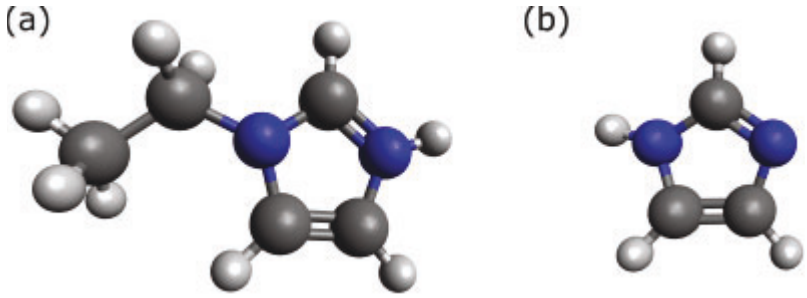

Figure 3: The structure of n-ethylimidazolium (a) and imidazole (b).

The relative strength of the acid-base pair in the PIL will determine how well the proton exchanges[9] and greater differences in pK_a values will lead to a greater percentage of the pairs gaining a charge. N-ethylimidazole and HTFSI can be combined to form a C_2HIm^+ and $TFSI^-$ PIL ($[C_2HIm^+][TFSI^-]$). HTFSI donates its proton to form C_2HIm^+ and $TFSI^-$,

which does not accept it back due to the low $\mathrm{p}K_\mathrm{a}$ of the conjugate acid. Therefore, the charges in the pure IL will undergo diffusion via vehicular transport.

ILs can be modified to encourage diffusion via the Grotthuss mechanism by adding solvents that are able to accept and donate hydrogen bonds. In previous studies, water and imidazole have both been tested as solvents to accept the excess proton.[9] In imidazolium-based systems, imidazole is able to solvate the IL better than water due to the similar organic properties of imidazole to the imidazolium-based IL, whereas water has a tendency to phase separate in such systems. Water is a common neutral solvent added to ILs, but organic solvents are more miscible in a $[C_2HIm^+][TFSI^-]$ IL and imidazole is ideal due to its similarities in structure, function, and $\mathrm{p}K_\mathrm{a}$ to C_2HIm.

1.3 Fuel Cells

Improving the proton transport in PILs can potentially lead to the development of more efficient fuel cells (Fig. 4). Hydrogen fuel cells (HFCs) require a source of hydrogen that can be oxidized at the anode to generate protons. The most common source of protons in HFCs is H_2. While the electrons create a current, the protons travel through an electrolytic fluid to the cathode where molecular oxygen is reduced by the electron and combines with the proton to create water waste. This process typically uses proton exchange membranes (PEMs) with added water to facilitate proton transfer. PEMs generally consist of an acidic polymer membrane between the cathode and the anode. The acidic protons on the polymer membrane transfer to water in the electrolyte layer and the protons travel through the water network via the Grotthuss mechanism. Upon

the protons reaching the cathode, they recombine with the electrons and oxygen to form water vapor, which allows for the fuel cell to expel harmless, clean waste.[10]

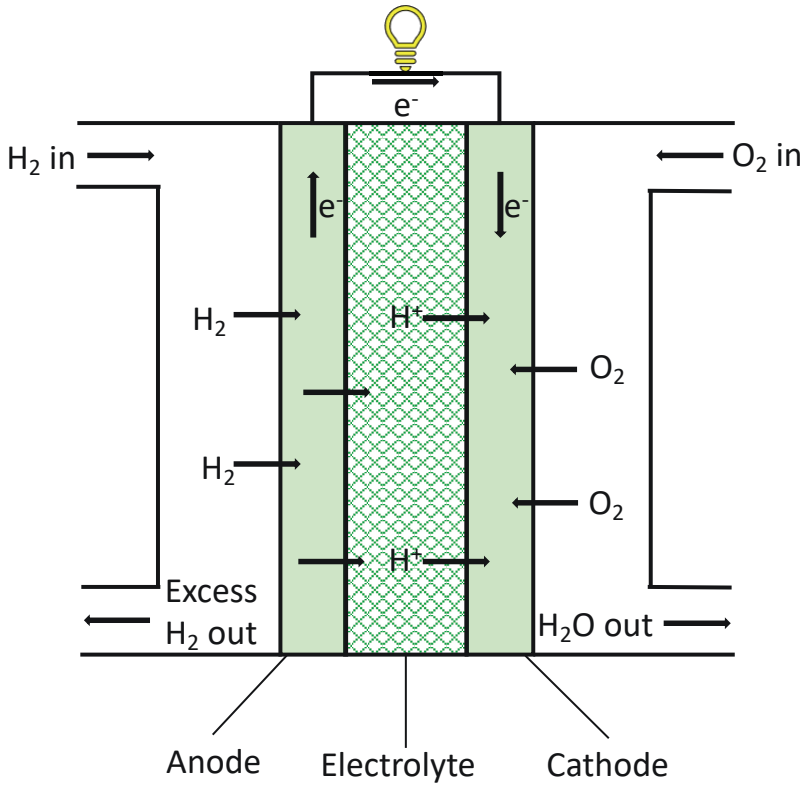

Figure 4: Fuel cell schematic. H_2 is pumped in at the anode and loses an electron. The proton then enters the electrolyte layer which is filled with electrolyte fluid to transfer the excess proton to the cathode while the electron performs work. At the cathode, the proton recombines with the electron and molecular oxygen to form water, which is secreted as harmless waste.

Although water is efficient at proton transport, it evaporates at elevated temperatures and must be replenished frequently in order to maintain proton conductivity. The transport of protons is vital to the function of fuel cells and research into better proton conductors is necessary. PILs can be useful in fuel cells because their use typically means that fuel cells can run at a higher range of temperatures, and the anhydrous properties of the imidazole systems can reduce the need for water in charge transport.

1.4 Imidazole systems

Imidazole analogues are heterocyclic species containing nitrogen and have been shown to form hydrogen bond networks as in water[11] and can therefore potentially participate in proton transfer. Imidazole analogues have been researched for their ability to accept and donate protons, otherwise known as "amphoteric properties." Imidazole has been studied in regard to its potential for proton diffusion in membranes and confined spaces, and previous work has shown that imidazole is a good proton conductor.[8, 9, 11, 12] Much like water molecules, imidazole's amphoteric properties allow it to form lengths of hydrogen bonded wires, similar to water networks, and potentially accept and donate protons when in the correct orientation and proximity. Understanding the mechanism of proton transport is vital for understanding and improving electrochemical systems.[13] Additionally, the understanding of proton transport mechanisms is of great interest to the scientific community.

Imidazole can become a cation or anion, or remain neutral, depending on how many hydrogens it accepts or donates. The standard imidazole ring consists of a five-member ring containing two nitrogen atoms. Each nitrogen has the potential to covalently bond or hydrogen bond to a proton, and the $\mathrm{p}K_{\mathrm{a}}$ value of the second proton is around 7 (intracellular pH), depending on the derivative. Different derivatives of imidazole are used for various purposes.[14] Unaltered imidazolium (where both nitrogen atoms possess a proton) is common in biochemical buffers used to remove histidine tags whereas benzimidazole is commonly used in various pharmacological applications and is a

common ingredient in many drugs such as antivirals, anticarcinogens, and antimicrobials.[15]

The temperature of the IL influences proton transfer. Pure imidazole has a melting point of 364 K, but when placed in an IL, the mixture is able to remain liquid at room temperature.[5] Upon the addition of too much imidazole, however, the imidazole rings will interact with each other instead of the IL and return to the solid phase. It has also been found that higher temperatures reduce the efficiency of the Grotthuss mechanism compared to the diffusion of other charges. As temperature increases, the other species move more and diffuse more quickly through the system.[12] Therefore, the temperature and concentration of an imidazole-solvated IL will determine the efficiency of charge diffusion.

An alternative way to create neutral species in an IL is through the addition of solvent instead of reducing the difference in $\mathrm{p}K_\mathrm{a}$ between the ion pairs. A surplus of imidazole added to HTFSI creates neutral imidazole species mixed with a [HIm^+][$TFSI^-$] IL. This allows for wires to form on either side of imidazolium and proton transfer is able to occur in both directions.[12] The formation of imidazole networks in [Im^+][$TFSI^-$] ILs is congruent with the high acidity of HTFSI. Thus, there is little interaction between $TFSI^-$ and the cation, which allows for Im^0 species to solvate the excess proton without competition from the anion.

Imidazole can be altered in various ways depending on the context in which it is being used. For instance, the $\mathrm{p}K_\mathrm{a}$ may be changed with the addition of different side chains of different electronegativities. Adding longer hydrophobic side chains can also

increase hydrophobicity of the entire molecule and adding these side chains to the nitrogen atoms can remove the amphoteric properties. Different side chains on the imidazole ring can also influence the size of the species which can affect the rate of diffusion. As a result, modifying imidazole can lead to a change in overall ionic conductivity.[11] $EMIM^+$ has been studied in regards to ILs with various modifications to the IL. Previously, an ionic liquid system containing $EMIM^+$ and acetate has been studied due to its strong hydrogen bonding capabilities where it was found a hydrogen bond can occur between the carbon at position 2 (Fig. 5) of $EMIM^+$ and the carboxylate group on acetate.[16]

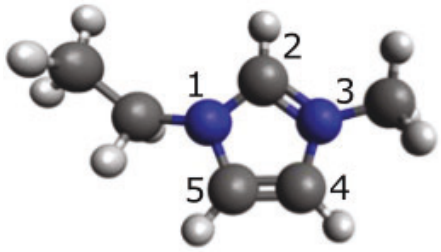

Figure 5: The positions of each atom on $EMIM^+$.

The formation of networks and ultimately proton transfer relies on the formation of strong hydrogen bonds between species. Hydrogen bonding occurs strongest at an angle of 180° between the donor, proton, and acceptor; to create the optimal position for imidazole to exist at an orientation where it can form a strong hydrogen bond for transport to occur. The amount of imidazole in the system also determines the mechanism by which charge is conducted and whether or not proton transfer is likely to occur.

Previous research[5] has further shown that the mole fraction (χ) of imidazole in $[C_2HIm^+][TFSI^-]$ PIL systems affects the mode of proton transport. In systems that contain

$\chi = 0.2$ Im^0 or less, bond networks form between the cation, solvent, and anion prohibiting charge diffusion via vehicular transport. Little charge transport is seen at low concentrations because not enough solvent is added to form Im^0 networks while the ions are prohibited from diffusing due to hydrogen bonding with the limited solvent. In systems containing concentrations greater than $\chi = 0.5$ of imidazole, greater vehicular transport is seen due to the bond rearrangement that occurs between $\chi = 0.2$ and $\chi = 0.5$ As more solvent is added, Im^0 species naturally begin forming bond networks as they are more likely to come into contact when greater amounts are added. This frees up the anion to diffuse via vehicular transport which becomes more prevalent at $\chi > 0.5$. However, the Grotthuss mechanism also becomes more prevalent as the imidazole wires form. In solvent concentrations greater than $\chi = 0.8$, the solution separates due to the tendency of imidazole-based species to aggregate. Without a solvent, $EMIM^+$ molecules have been known to stack on each other due to the π-bonds in the ring and the hydrophobic ethyl chain.[16] Likewise, imidazole solvents will also aggregate rendering high concentrations of imidazole unable to solvate.

In this particular study, the cation (C_2HIm^+), was chosen due to the prevalence of imidazolium analogues in literature. Previous studies[4,16,17] have used $EMIM^+$ in ionic liquid research due to its high charge conductivity,[17] although $EMIM^+$ is aprotic. For the purposes of this study, C_2HIm^+ was used instead because it has the potential to transfer an acidic proton but is structurally similar to the well-characterized $EMIM^+$ with the methyl substitute simply changed to a proton.

1.5 Solvate Systems

Proton transport was further studied in a system containing hydronium solvated by 18-crown-6-ether (18C6) and $TFSI^-$, as seen in Fig. 6. Together, 18C6 and hydronium formed a complex, and water was added as a solvent. Such a system is called a "solvate system" or a "solvate ionic liquid (SIL)" due to the solvated acid-base complex[13, 18] SILs are a relatively new addition to IL research, but their properties are intriguing for a number of applications. Traditional ILs often consist of weakly acidic and weakly basic ion pairs which coordinate but never strongly interact, and there are few instances otherwise. SILs allow for stronger acids or bases to be used in ILs despite to their high melting points. ILs

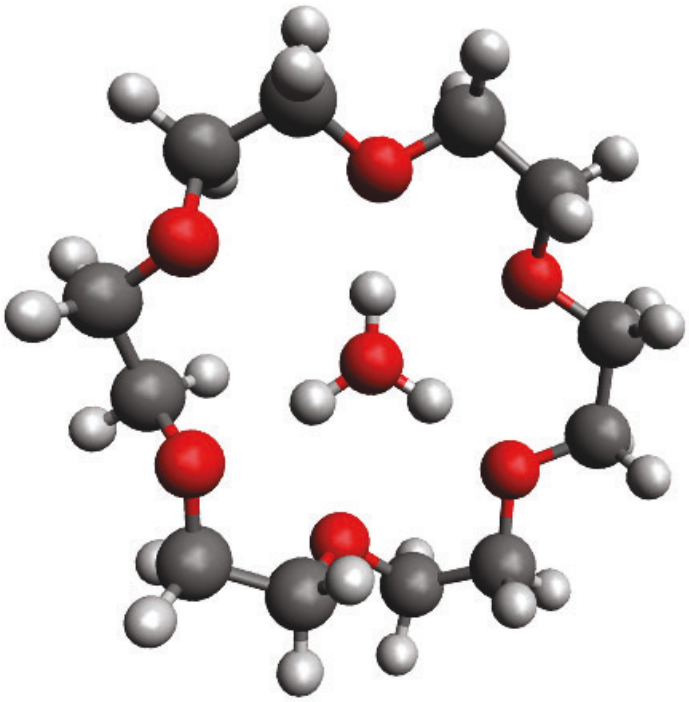

Figure 6: A solvate system consisting of 18-crown-6-ether solvating hydronium.

with high melting points are considered molten salts instead of RTILs but a solvation shell allows for strong acids and bases to be used in ILs at lower temperatures.[19]

SILs can be applied to lithium-ion batteries. Li^+ has high Lewis acidity. This leads to high viscosity and ionicity with low conduction at room temperature. By pairing Li^+ with a strong Lewis base, the acidity of Li^+ has been found to decrease and can conduct a charge more rapidly and at lower temperatures which can increase the efficiency of lithium-ion batteries. Ethers are typically used to counter strong Lewis acids such as lithium as they can be categorized as strong Lewis bases.[19] By pairing strong Lewis acids with strong Lewis bases to form complexes, the resulting system behaves very similarly to RTILs.

We hypothesized that proton exchange was possible between the solvated hydronium and its conjugate base since water is known to be able to accept and donate protons. It easily forms hydrogen bond networks that allow for the exchange of protons via the Grotthuss mechanism with little displacement of nuclear coordinates. This is much higher than the diffusion of most ions through a system. Previous research has shown that proton exchange is possible between the hydronium-18C6 complex and other species.[13] Furthermore, it was found that neutral species could be added to the IL to accept the proton from hydronium. For instance, deionized water can be added to transfer the proton on hydronium.

Additionally, previous research has demonstrated that water can act as a bridging molecule in IL systems.[16] When added to an [EMIM][Acetate] system, water was shown to form a bridge between two acetate ions. Although acetate was more strongly coordinated to the cation than water, water formed strong hydrogen bond networks with

each other and with acetate ions. These clusters of one water coordinated to two acetate molecules were prevalent when a moderate amount of water was added to the system. Upon increasing the amount of added water, however, a hydration shell formed around single acetate ions. The strong hydrogen bond networks of water and its capability to form a bridge between species make it ideal for proton transfer in PILs. Thus, SILs are of interest in studying charge diffusion.

2. Methodology

All three projects contained a set number of ion pairs and varying concentrations of added solvent. The initial configuration of the systems was determined using PACKMOL[20] to randomly place species in a simulation box with an initial approximate density near the target density where the initial density had to be reasonably close to the true density for the results to converge. The systems were equilibrated for 10 ns using LAMMPS under constant pressure and temperature. This allowed for a change in density from the estimated initial densities and the true densities of the systems were determined from the last 5 ns. This equilibration was run classically, so there was no bond breakage and formation. The volume of the simulation box was then calculated from the optimized density of the system, and classical MD was run again under constant temperature and volume. The purpose of the forcefields is to set the parameters for the electronic distribution of the ions, the bond angles, and rotational energies. For this study, the Canongia, Lopes, and Padua (CL&P) force field was used to describe the ions[21], the optimized potentials for liquid systems (OPLS) force field was used for imidazole species[22], and SPC/Fw was used for water[23]. The valence electrons were simulated using a TVZ2P basis set, the GTH core potential, and the Grimme correlation.

The final frame of the classical equilibration was used as the input for AIMD. Each simulation was run equilibrated with AIMD for 20 ps using CP2K[24], followed by 80 ps of production-level runs. Each system was run in duplicate starting from a different initial configuration. Unlike classical molecular dynamics simulations, bonds can be broken and

formed based on thermodynamic stability. AIMD is a more accurate method to study systems involving proton transfer than classical MD since proton transfer is an inherently quantum mechanical process due to the breakage and reformation of bonds.

3. C_2HIm^+ Systems

Imidazole was added to a system containing 16 pairs of the IL in varying concentrations: pure ($\chi = 0$), 8 species ($\chi = 0.33$), 16 species ($\chi = 0.50$), and 32 species ($\chi = 0.67$) to determine how the mechanism of proton transfer and charge diffusion differed with concentration of solvent, as the concentration of solvent has been shown to impact proton transfer. Each simulation was run at a constant temperature of 343 K and two different ion pairs were used: the first system consisted of C_2HIm^+ and $TFSI^-$ ($[C_2HIm^+][TFSI^-]$), and the second consisted of C_2HIm^+ and acetate ($[C_2HIm^+]$[Acetate]), the structures of which can be seen in Fig. 7. The systems were run under the same conditions

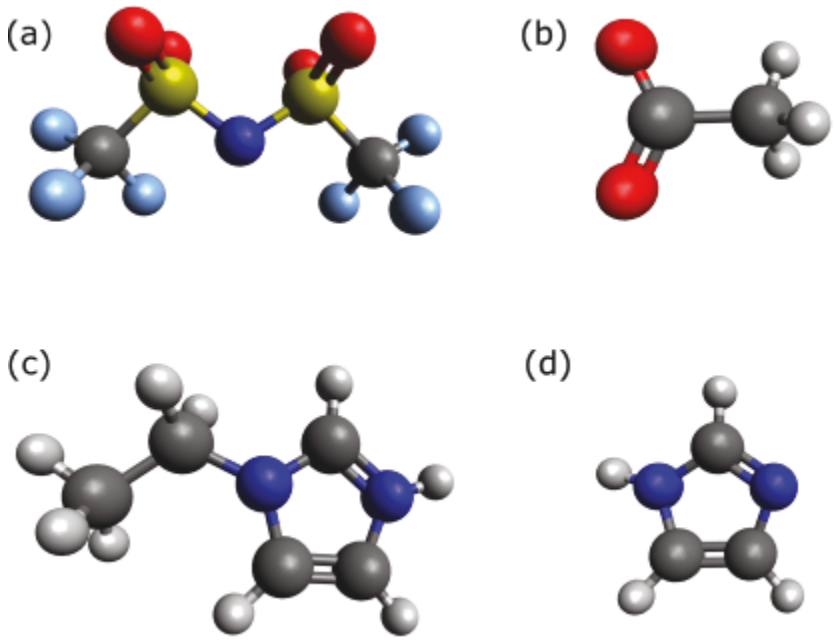

Figure 7: The structures of TFSI (a), acetate (b), C_2HIm (c), and imidazole (d).

and with identical concentrations of added solvent, with the only difference between the two being the anion, to determine how the anion affects proton transport.

To determine the structure of the ILs, the RDFs of each system was calculated as described in Fig. 8. This allowed for a greater understanding of solvation structure around select molecules which can be used to determine the species on which a proton may reside at some point in the simulation. The RDF also grants insight into the overall structure of the IL.

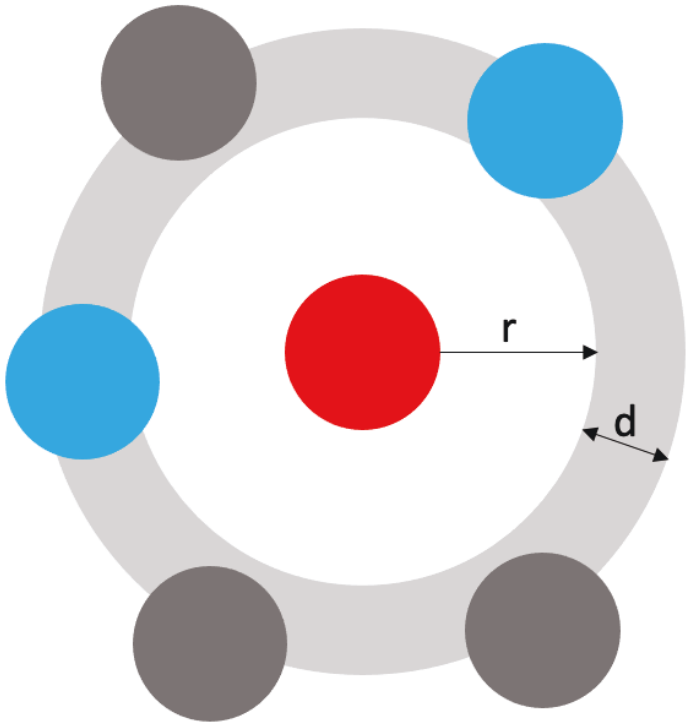

Figure 8: The radial distribution function (RDF) shows the solvation structure around a selected species. At each radius (r) from the species (red), a shell of a fixed width (d) is analyzed for the presence of the second species (blue) to determine how many of the second species solvate the first species at each radius. Other species in that solvation shell are not taken into account and their RDFs must be calculated separately. Likewise, any species outside of d is not taken into account.

3.1 Acetate

The acetate system was only run for the 20 ps of equilibration and the project was discarded before production-level simulations could be run. The system did not demonstrate ideal charge conduction, so no further experiments were completed. The RDFs between the acidic proton and either imidazole or acetate are shown in Fig. 9. In each system, the excess proton is completely transferred to acetate as shown in the peak centered at 1.10 Å. Another peak centers at 1.55 Å showing hydrogen bonding between the proton and the second oxygen on acetate, however the proton is unable to transfer directly to the second oxygen due to binding to the first. Additionally, the proton is solvated by other acetate species via hydrogen bonding as shown by the peak centered at 2.50 Å. In contrast, the solvation of the proton (H_{Im}^{+}) by the nitrogen on imidazole (N_{Im}^{0})

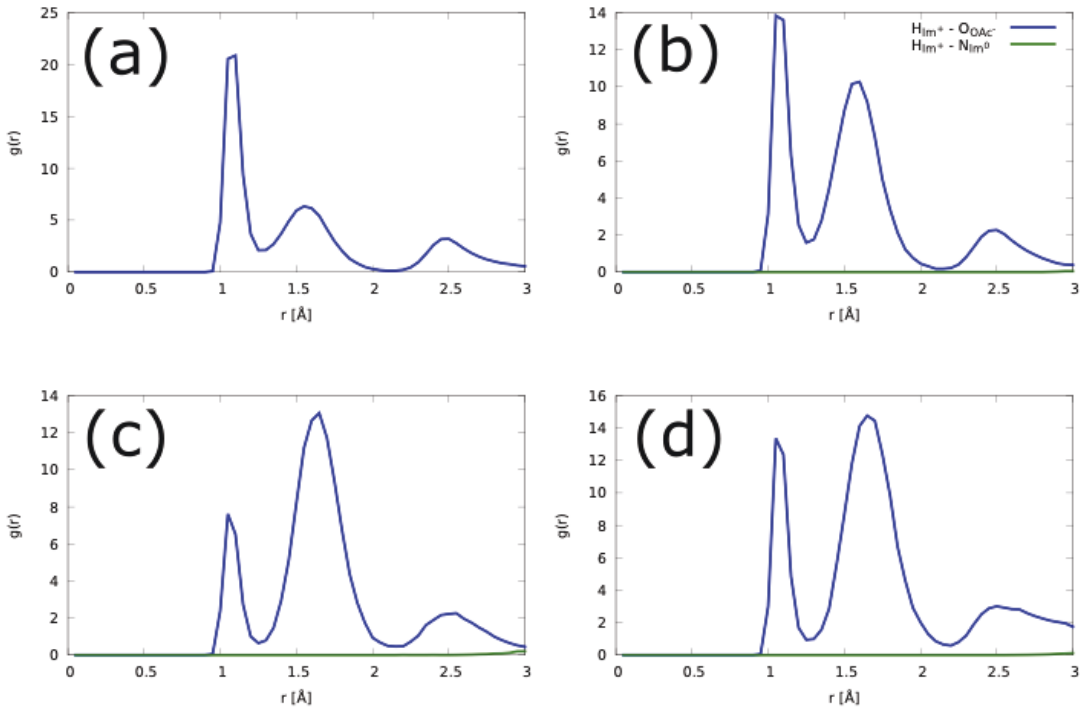

Figure 9: RDF of H_{Im}^{+} to acetate and N_{Im}^{0}.

is nonexistent. The solvation structure was completely dominated by acetate so that imidazole appeared as a line at the bottom of the graph with no discernable peaks. The lack of any substantial N_{Im}^{0} peak in the RDF indicates that despite the presence of imidazole, it does not interact with the proton. Due to the high pK_a of acetic acid, acetate accepted the proton from Im^+ when proton transfer occurred in every instance as seen in Fig. 10. The coordination number was calculated by integrating the RDF and shows that 100% of protons were solvated by acetate.

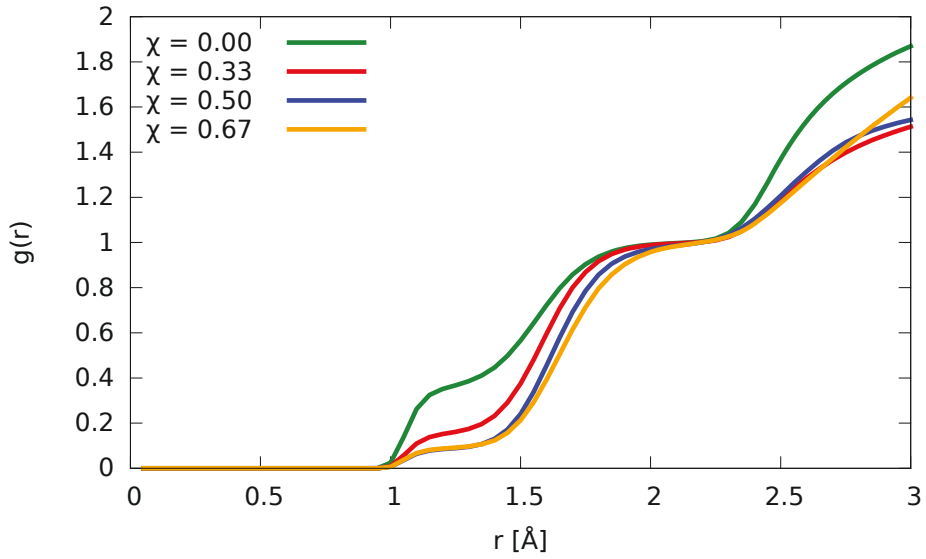

Figure 10: The coordination number of H_{Im}^{+} to acetate.

The total number of proton hops per ps was calculated for each system as shown in Table 2. The number of hops was indirectly related to the mole fraction of imidazole: $\chi = 0.00$ showed the most hops indicating H_{Im}^{+} was transferred between the pure IL pairs. This concurs with the RDF which showed acetate dominating the solvation structure of the proton. However, ownership of the proton decreased with increased additions of imidazole. In other words, the addition of imidazole quenched proton transfer.

Table 2: Total proton hops in each mole fraction of Im^0.

Mole Fraction of Imidazole	Hops/ps
0.00	69.95
0.33	42.30
0.50	22.95
0.67	20.80

It was found that the anion hydrogen bonds with the cation and the proton rattles between the two species. Because of this configuration, sequential forward hopping was unlikely to occur as C_2HIm is unable to simultaneously accept and donate a proton. Wires of acetate did not form as the acetate species interacted more favorably with the cation. An example of such interaction is shown in Fig. 11. Thus, the mechanism of proton transport in this system is more likely to occur via vehicular transport. Upon the addition of imidazole, proton transfer among the ion pairs was shut down. A decrease in proton hops was recorded in Table 2, directly correlating to increasing additions of imidazole.

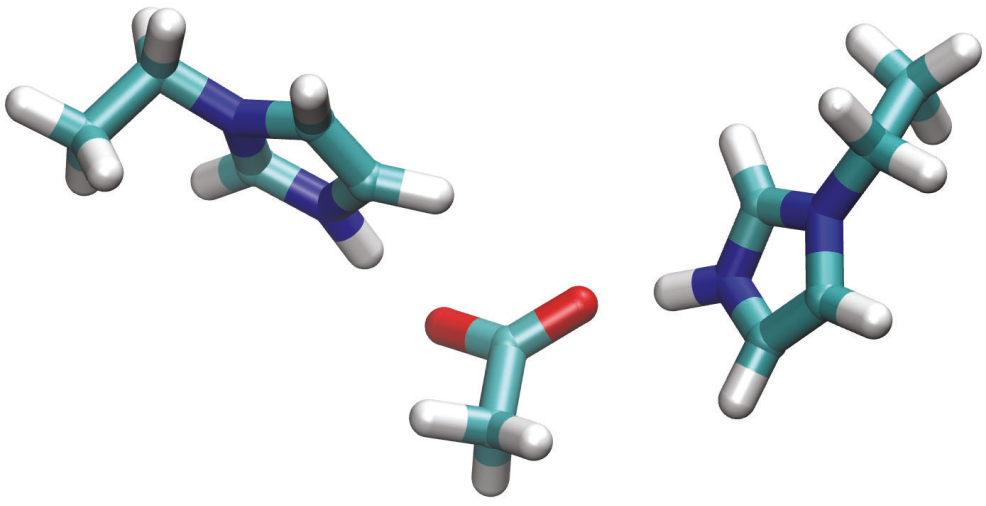

Figure 11: Both oxygens on an acetate anion solvated by two C_2HIm species.

3.2 $TFSI^-$

Unlike the acetate system, adding imidazole to the $[C_2HIm^+][TFSI^-]$ system facilitated proton hopping as was seen in the hopping trend in Table 3. The system without any solvent did not show any hopping but as imidazole was added, hopping increased. For this reason, we further explored proton diffusion in these systems.

Table 3: The total proton hops in each mole fraction of imidazole.

Mole Fraction of Imidazole	Hops/ps
0.00	0.00
0.33	3.28
0.50	7.38
0.67	10.28

Using the scheme outlined in Chapter 2, the computationally-determined densities of the systems closely followed those determined by experiment. The simulations were run at 343 K to study the IL at an elevated temperature, but the experimental work was performed at 303 K and had a higher density than the theoretical densities determined at 343 K. We also calculated our densities for the same system at 303 K, and the results are very similar to the experimental values.[5] Therefore, the densities for the identical system at 343 K are reliable. A comparison of experimentally and computationally determined densities is shown in Fig. 12.

The diffusion of the various ionic and molecular species was defined based on the center of mass (CoM) or the center of ring (CoR) when applicable. By calculating the diffusion of the center of the species, the movement of the entire molecule as a whole

can be determined. The CoM was used for $TFSI^-$ and the CoR was used for C_2HIm^+ and imidazole.

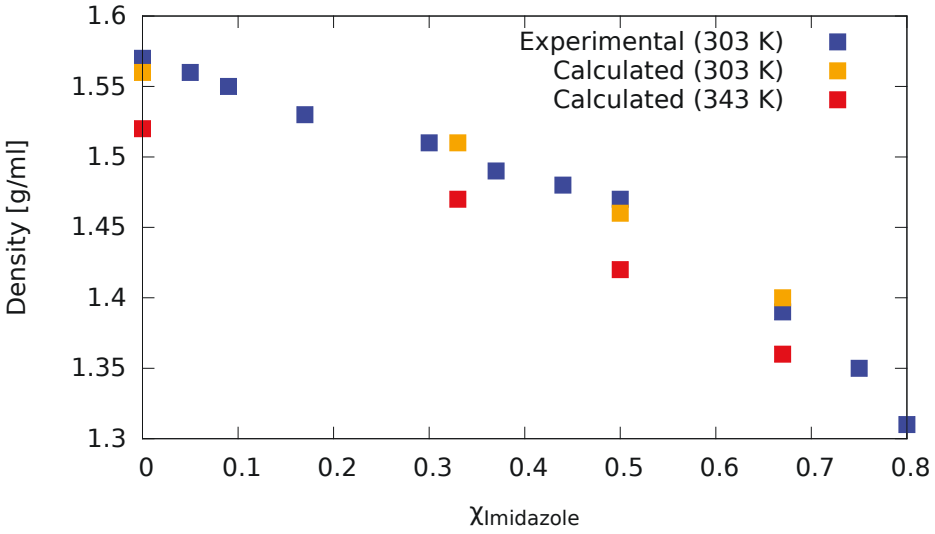

Figure 12: Densities of experimental systems versus our simulations.[5]

Through imidazole's participation in Grotthuss hopping, the excess proton was able to transport across the system via hydrogen bond networks and as a result, charge migration occurred via hopping along imidazole wires. Charge diffusion was calculated along the wire beginning at the cation; an example of such diffusion is shown in Fig. 13. The charge can be seen on the first position of the imidazole ring in Fig. 13(a) where an excess proton was bound at timestep 41889. The charge existed primarily on the nitrogen directly before the proton hops to the adjacent imidazole at timestep 41890. Over the course of 146.5 fs, the charge diffused across the center of the imidazole ring and hopped to the third imidazole at timestep 42184.

The mean squared displacement (MSD) shows the average displacement of a species over time. The MSD was calculated using the sum of the difference in displacement of a species at each timestep:

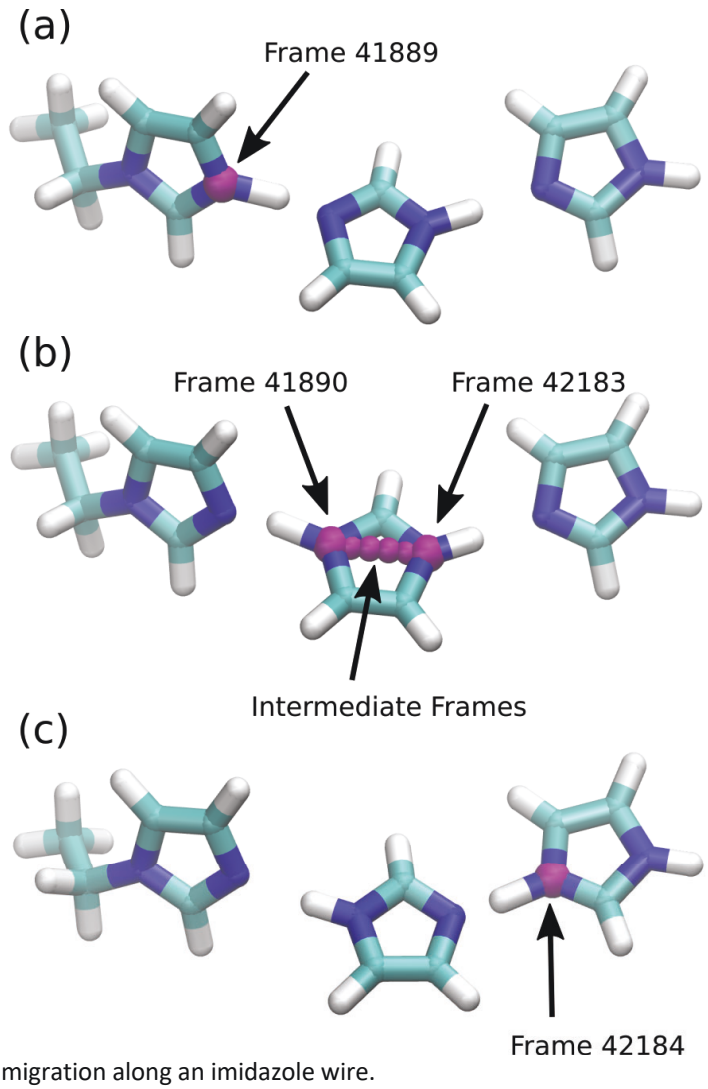

Figure 13: Charge migration along an imidazole wire.

This was averaged by the total number of species to create the graph in Fig. 14. According to the Einstein relation in Eq. 2, the diffusion of a species is directly proportional to the slope of the line. A steeper slope indicates higher diffusion with the three-

dimensional nature of diffusion taken into account. Due to rattling events, the MSD of the charge does not appear completely smooth but the general trend indicates overall diffusion that surpasses the diffusion of the other species. The positive charge had the highest MSD as it was able to travel very quickly along the imidazole wires via Grotthuss hopping. This is evidenced by the fact that the charge diffusion exceeds that of the excess protons themselves and the parent ions.

$$MSD(t) = \frac{1}{n}\sum_{i=1}^{n}|r_i(t) - r_i(t_0)|^2 \quad (1)$$

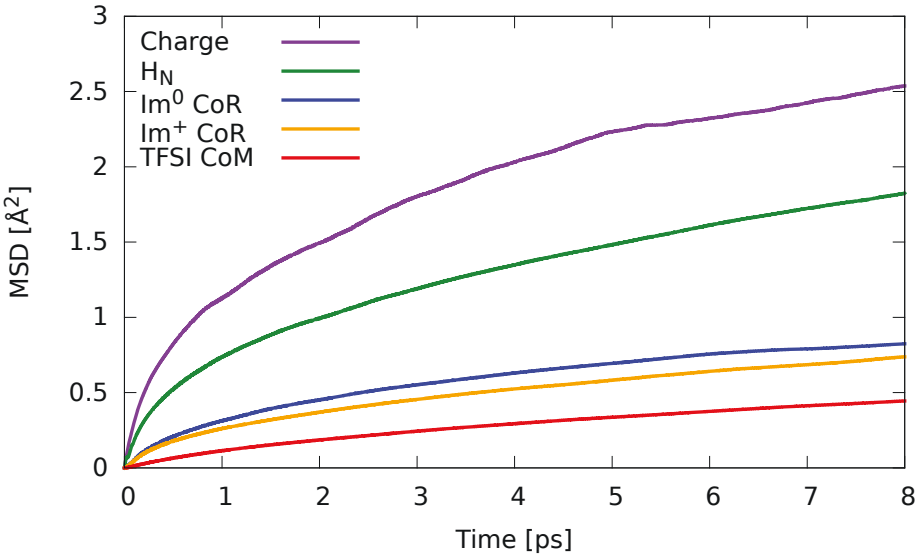

Figure 14: MSD of species in the χ = 0.5 system.

When the slope of the MSD was calculated, the diffusion coefficient of each species could be extrapolated and graphed in Fig. 15 to determine how diffusion changes with increased amounts of imidazole.

$$D = \lim_{t\to\infty} \frac{\mathrm{MSD}(t)}{6t} \tag{2}$$

Charge diffusion increases with increasing mole fractions of imidazole. Little variation of diffusion occurred among the other species as imidazole was increased. Added solvent therefore had no effect on diffusion via vehicular transport. However, diffusion of the charge increased as more imidazole became available to conduct a charge indicating that a different mechanism is responsible for the charge diffusion. As the amount of imidazole was increased, more species became available to form hydrogen-bonded networks allowing the proton to hop from one species to the next via the Grotthuss mechanism. Because of the rapid diffusion the Grotthuss mechanism allows for in comparison to vehicular transport, the diffusion of the charge increased substantially

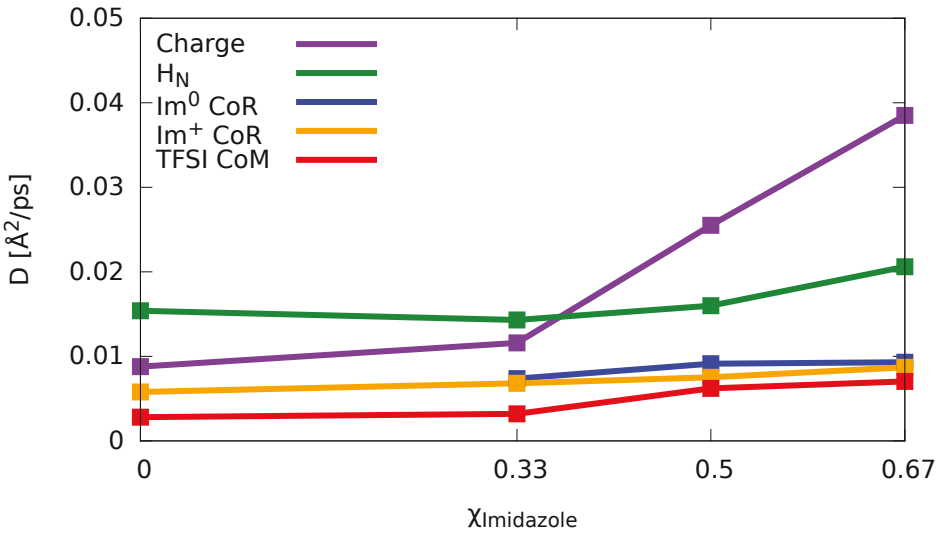

Figure 15: Diffusion of species by mole fraction of imidazole.

when more wires were able to form. Chances of imidazole species forming the correct orientation and proximity to accept a proton also increases and longer wires can form.

More cations are able to relinquish their proton and protons are able to travel farther with increased concentrations of imidazole. This contributes to a drastic increase in charge diffusion in relation to the diffusion of other individual species.

Fig. 16 depicts the RDF between H_{Im}^+ and the different species it can interact with. Therefore, the solvation structure of an excess proton attached to Im^+ can be deduced based on its surroundings. Due to the hydrogen bonding-capability of the anion, the interaction between the acidic proton to $TFSI^-$ was also analyzed and compared to the solvation structure of the proton to imidazole for each system. HTFSI is too acidic to accept a proton and only weakly solvates the proton compared to imidazole. This pattern is seen in all three systems.

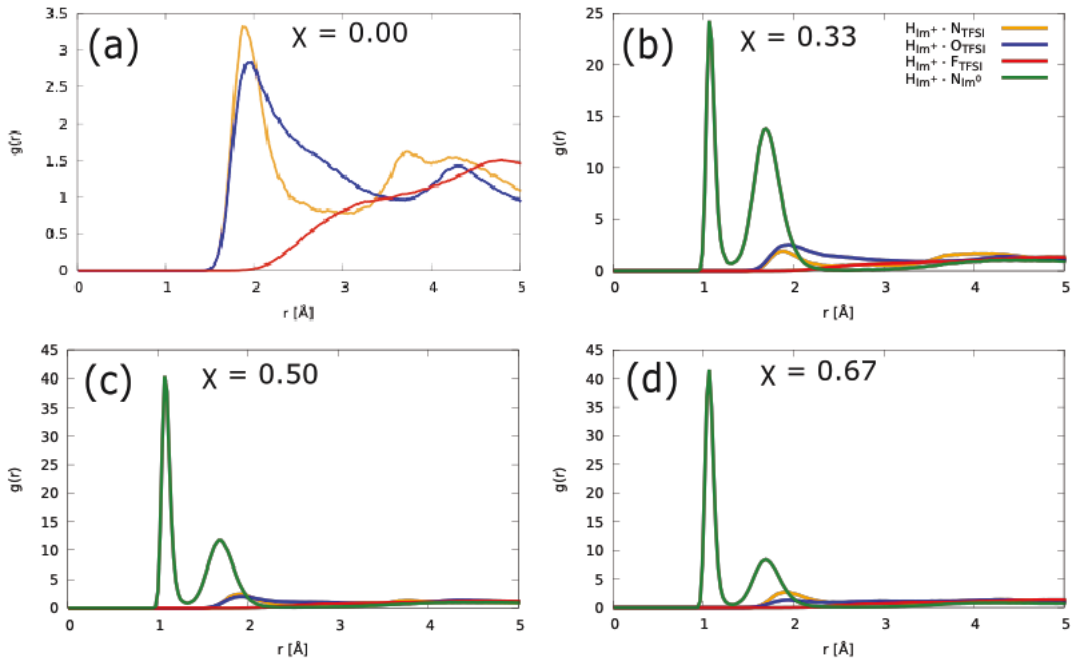

Figure 16: The RDF of imidazolium to NIm^+, O_{TFSI}, N_{TFSI}, and F_{TFSI}.

Of the potential hydrogen-binding species in the anion, oxygen has the strongest interaction with the acidic proton. Oxygen can be seen weakly solvating the cation at a peak centered at 2.07 Å in all the systems. Nitrogen can also be seen solvating the cation

weakly at a peak centered at 1.95 Å, however fluorine does not seem to form any discernable solvation structure. Amounts of fluorine species around the cation rises as the distance increases, however, there are no discernable peaks signifying a specific solvation structure. More likely, the fluorine species are in solution surrounding the imidazole, but not particularly interacting with the charge.

Next, the RDF between HIm^+ and N_{Im}^0 was analyzed for all systems in Fig. 17. A peak at 1.08 Å in all systems indicates the acidic proton is 1.08 Å from an imidazole nitrogen, which is the length of a covalent bond. This indicates the proton has hopped to the subsequent species and imidazole has ownership of the proton. As the mole fraction of imidazole increases, so does the ownership of the acidic proton. The peak centered at 1.68 Å in all systems indicates hydrogen bonding. The imidazole is hydrogen bonding with the acidic proton at that distance which gives the proton potential to hop to the solvating imidazole.

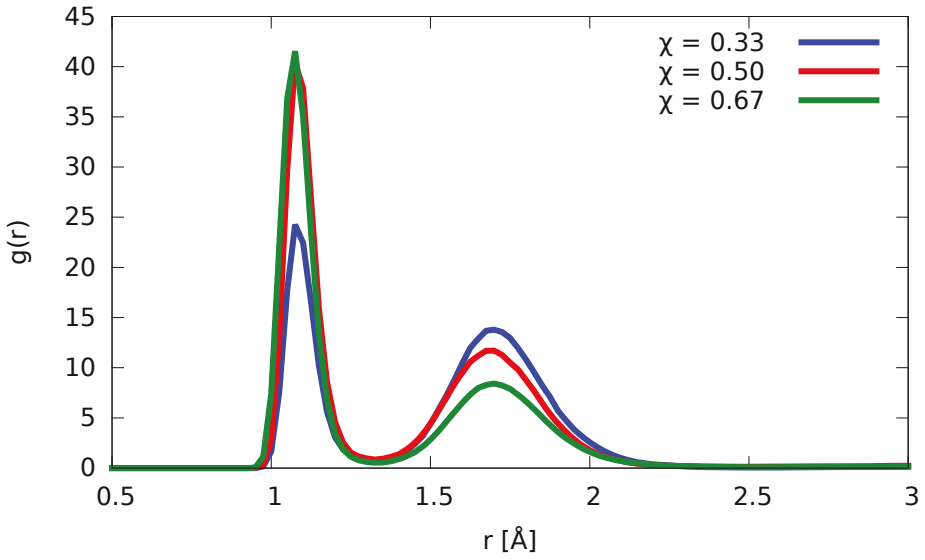

Figure 17: The RDF of the acidic proton on Im^+ to N_{Im}^0 in all systems.

The coordination number was found by integrating the RDF in Fig. 17 to create the graph in Fig. 18. The coordination number determined the amount of HIm^+ species that were solvated by NIm^0. The coordination number increased as the concentration of added imidazole increased since more available solvent allowed for increased chances of coordination with HIm^+. The most coordination occurred in the system where $\chi = 0.67$. There, the acidic protons were bound to imidazole species 23% of the time as indicated by the plateau beginning at 1.13 Å. This is more than $\chi = 0.50$ where imidazole has ownership of the proton 13% of the time. The system where $\chi = 0.33$ has the least amount of proton ownership at 5%. A second plateau beginning at 2.50 Å occurs where hydrogen bonding is prevalent. At this distance, 61% of the $\chi = 0.67$ is solvated by imidazole species. 44% of Im^+ protons are solvated in the $\chi = 0.50$ system and only 25% are solvated in the $\chi = 0.33$ system.

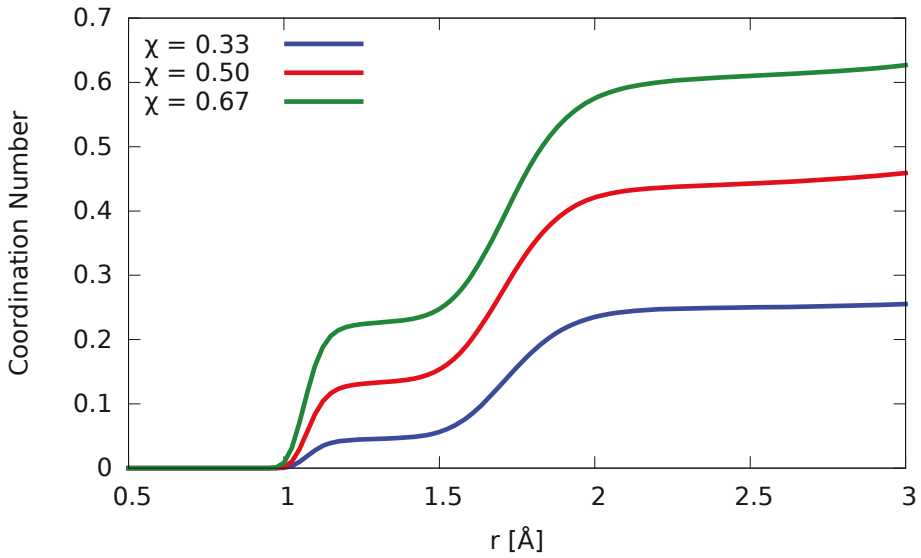

Figure 18: The coordination number of $N_{Im}{}^0$ solvating $H_{Im}{}^+$.

The concentration of added imidazole impacted the solvation of the cation because for a proton to transfer from the cation to an imidazole species, the orientation and proximity of the proton and imidazole species must align. Hydrogen bonding is strongest at 180°, therefore, the proton must align with the accepting nitrogen of imidazole at 180° in order to form a bond strong enough to initiate transfer. Additionally, the two species must be in close proximity in order for hydrogen bonding and transfer to occur. The systems containing higher concentrations of imidazole therefore have an increased chance of achieving both conditions for proton transfer. Therefore, higher concentrations of imidazole will result in greater occurrence of proton transfer.

The solvation structure around transferrable protons on HIm^0 was also analyzed due to imidazole's ability to form wires. When the excess proton hops to Im^0, the charge has the potential to diffuse across the ring and hop to a secondary species via the Grotthuss mechanism. Therefore, it was important to determine the solvation structure around $H_{Im}{}^0$ as well. As with the RDF of $H_{Im}{}^+$, the solvation of each atom with hydrogen bond capabilities were analyzed. This included other Im^0 species as well as the oxygen, nitrogen, and fluorine on the anion.

In all systems, $TFSI^-$ was shown to solvate H_{Im}^0 weakly but never accepts a proton. Oxygen (O_{TFSI}) was shown to have the strongest affinity for H_{Im}^0 at 1.63 Å followed by nitrogen (N_{TFSI}) at 2.03 Å. Fluorine (F_{TFSI}) appears in the RDF due to its presence on each TFSI- molecule, but F_{TFSI} never displayed a distinct peak in the RDF which indicates that F_{TFSI} does not interact with H_{Im}^0. The χ = 0.33 system RDF does not show an ownership

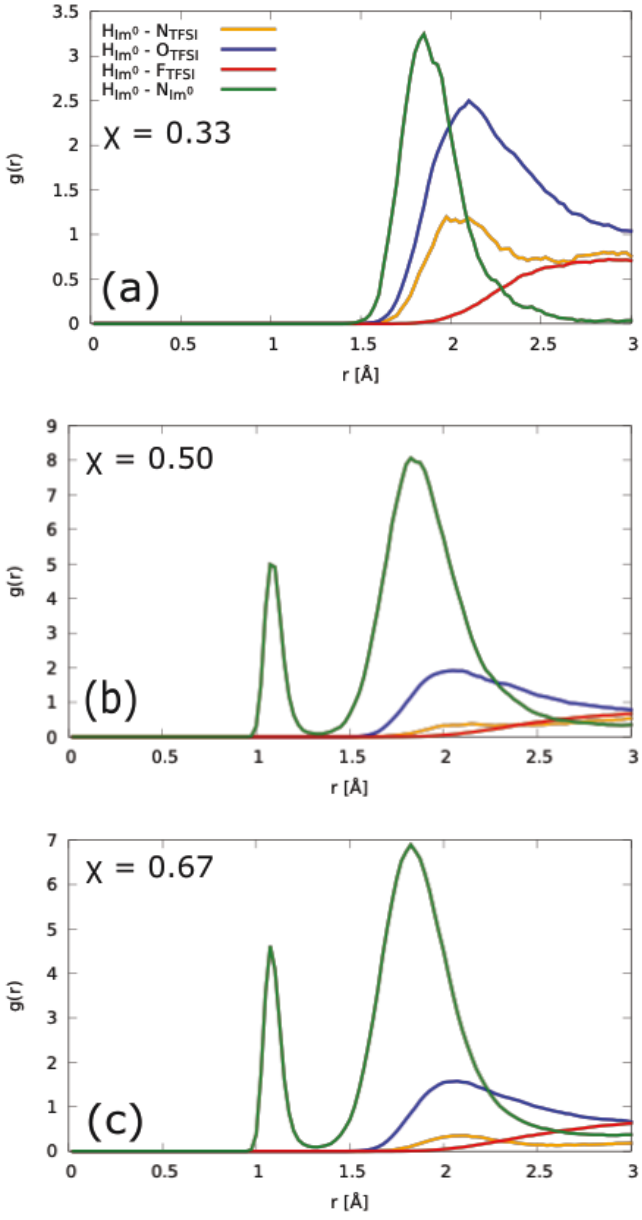

Figure 19: The RDF of H_{im}^0 to the system.

peak, indicating that subsequent Im^0 species did not accept the proton, so no secondary hopping occurred. However, the solvation of Im^0 around $H_{Im}{}^0$ was stronger than the solvation of $TFSI^-$.

Previous research has shown that $TFSI^-$ is too acidic to accept the proton from the cation. This phenomenon is displayed in the RDFs of all three systems with various concentrations of imidazole added. The added imidazole has a much higher affinity toward the cation than $TFSI^-$ which displays only weak solvation and no ownership of the acidic proton. The anion therefore did not interfere with the formation of wires and the ultimate transport of charge.

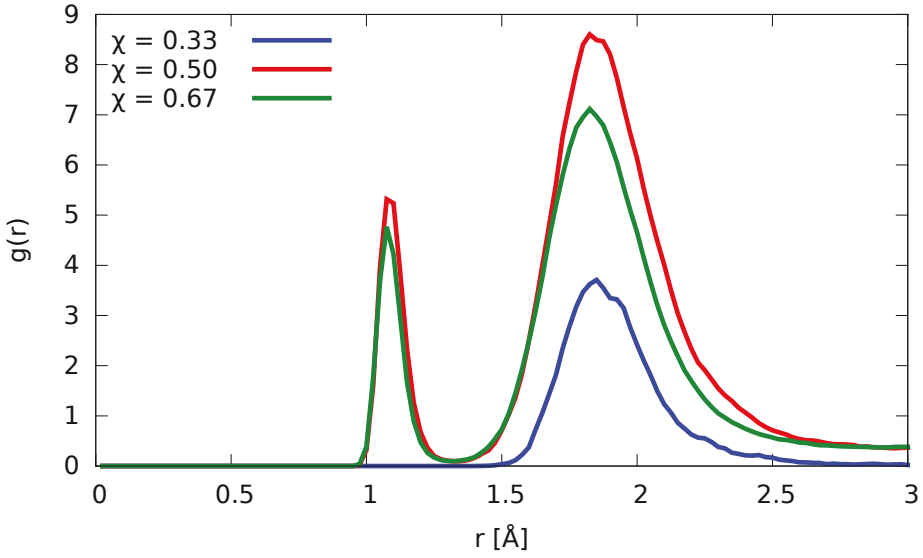

Figure 20: The RDF of $H_{Im}{}^0$ to other Im^0 species.

The solvation structure of $H_{Im}{}^0$ to $N_{Im}{}^0$ in the $\chi = 0.50$ and $\chi = 0.67$ systems showed that $H_{Im}{}^0$ hops to subsequent imidazole molecules after the initial transfer from Im^+ due the presence of an ownership peak at 1.10 Å. The increased amount of solvent available allows for a greater chance that the correct orientation and proximity will occur

between imidazole molecules to create networks. Thus, a greater concentration of imidazole allows for more opportunities for secondary hopping.

Fewer than 10% of H_{Im}^{0} coordinate to other Im^{0}s. Ownership is observed in the $\chi = 0.50$ and $\chi = 0.67$ systems as shown in Fig. 21. No ownership is seen in the $\chi = 0.33$ system and only small amounts of hydrogen bonding can be seen. This is due to $\chi = 0.33$ having fewer imidazole species to orient around a cation.

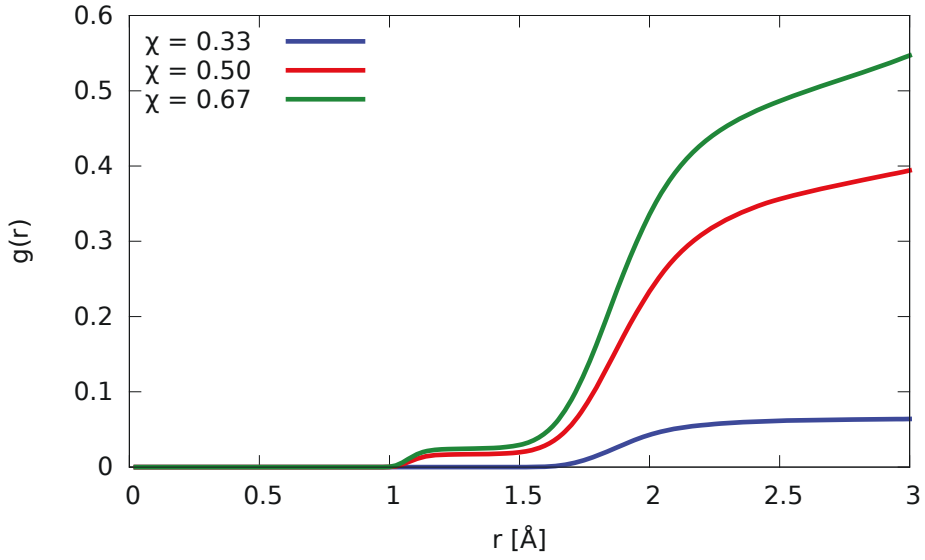

Figure 21: The coordination number of imidazole species solvating Im^{0} .

Based on the RDF data alone, the lengths of the imidazole wires formed remained uncertain. Further analysis of the imidazole wires was done to determine this, and a wide range of different wire lengths formed depending on the amount of solvent added and the initial placement of the molecules. As shown in Fig. 22, wires more than 6 species long were found in the $\chi = 0.50$ and $\chi = 0.67$ systems, but these wires were not common. As wire length increased, their prevalence in the simulations decreased. In the $\chi = 0.33$ system, wire length above 2 species was not seen and In the $\chi = 0.67$ system, however, wire lengths of 5 species were observed.

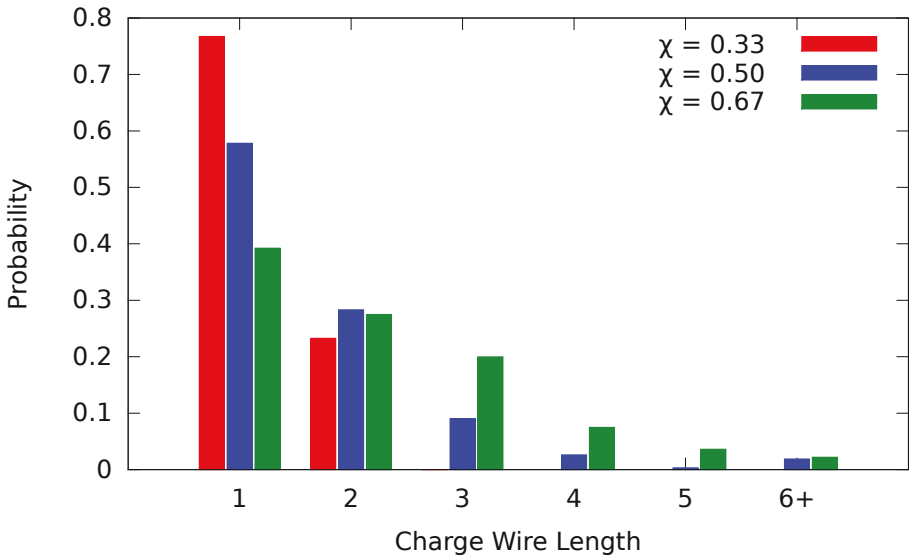

Figure 22: The probability of the number of imidazole species that will form in a wire based on mole fraction.

An example of an imidazole wire is shown in Fig. 23 transports a charge across four Im^0 before turning around and carrying the charge back to Im^+. The nitrogen atoms possessing the charge are highlighted in red to demonstrate charge diffusion as the proton hops. The transport from Im^+ to the third Im^0 takes place between 20-22 ps of the simulation. Between transfer events, "rattling" occurs as protons hop from one species to another and then back onto the original donor so that charge diffusion neither occurs at a constant rate nor strictly linearly. At 20000 fs, the proton is attached to Im^+ and transfer occurs at 21013 fs. From there, rapid concerted transfer occurs at 21159 fs. At

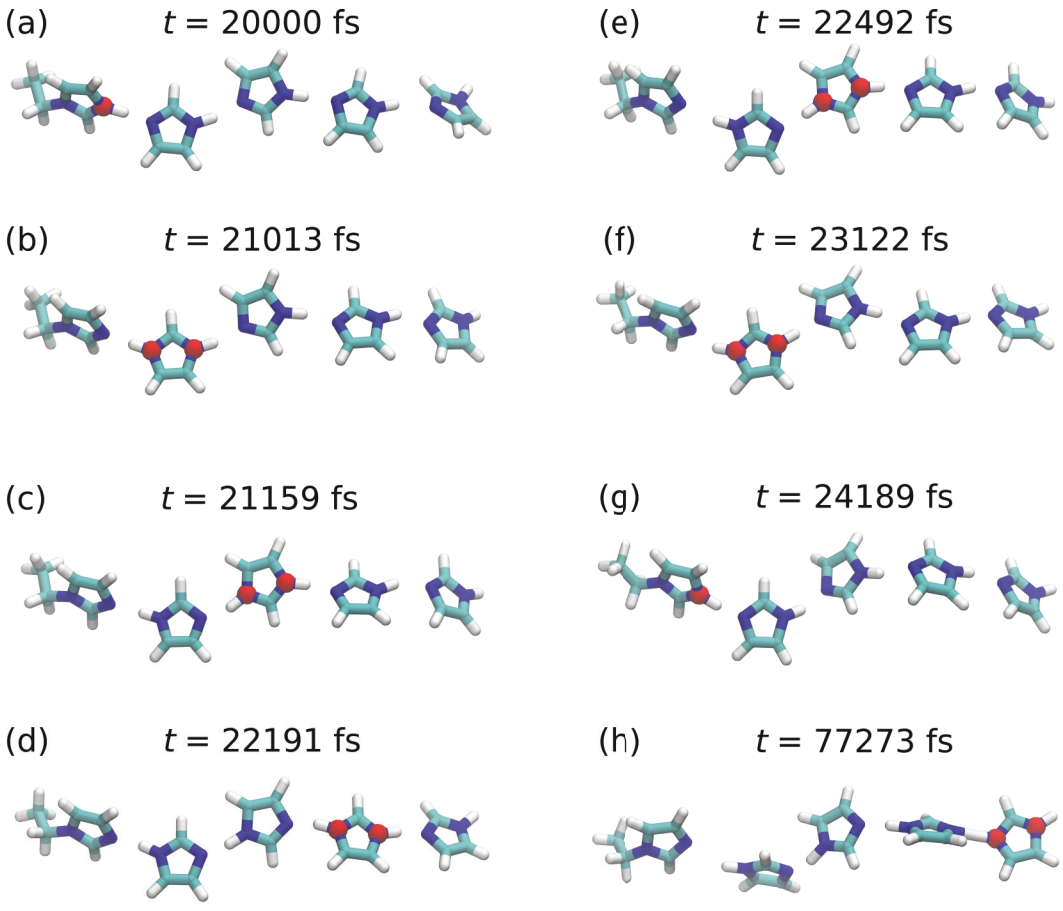

Figure 23: Proton hopping along a wire in $\chi = 0.67$ with the charge labeled red.

22191 fs, the proton reaches the fourth imidazole species. This consecutive hop occurs as a proton transfers to the second Im^0 only 117 fs later causes a quick diffusion of charge. From there, the direction of proton transfer reversed and the proton was transported all the way back to Im^+. Eventually, the proton was transported to the last Im^0 in the wire but the change in direction was due to the amphoteric properties of imidazole allowing for charge diffusion to occur in either direction. Because C_2HIm has an ethyl group substituting one of the nitrogen atoms, it is only able to transfer a proton in one direction and therefore serves as the "cap" to the wire, preventing charge transfer in the other direction. The proton hops occur consecutively to create rapid diffusion as the charge transfers across the system. This rapid diffusion of charge is due to imidazole's ability to undergo the Grotthuss mechanism. Although the charge diffuses quickly and proton hops occur in a manner of fs, the orientation of the parent species changes minimally over time. The diffusion of the proton alone is much quicker than the diffusion of the individual parent species.

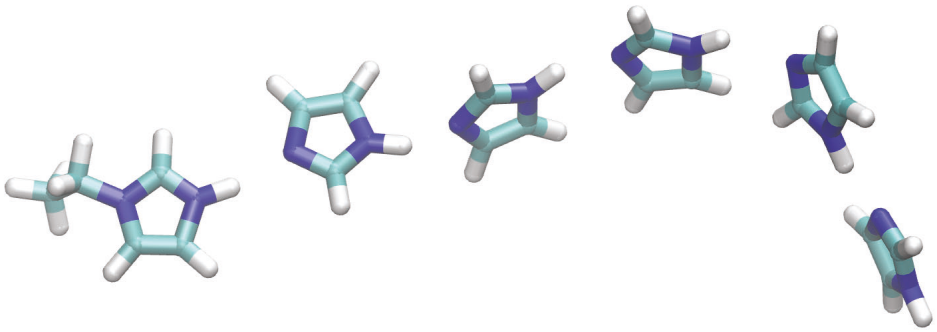

Figure 24: A wire of imidazole found in $\chi = 0.67$.

The $\chi = 0.67$ system showed the most wire formation as there is the most available imidazole in this system. This coincides with previous research which has

indicated that the more imidazole available, the more the charge will transfer via proton exchange. However varying wire formations occurred due to the species being placed in the simulation at random coordinates. Wire formation depended on the proximity and orientation of imidazole. Additionally, it is possible that wire formations to change as species re-orient throughout time. On the timescale these simulations are run (80 ps), enough time does not pass to see much re-orientation.

The potential mean force (PMF) in Fig. 25 describes the energy barrier a proton must overcome to transfer. The proton exists at the most thermodynamically stable position on its parent species. However, the transfer to a nitrogen on a different species requires the proton to overcome an energy barrier since it is more stable in a covalent bond than existing alone. To transfer, the proton must momentarily exist between the two species and this is the energy barrier that must be overcome for proton transfer to occur.

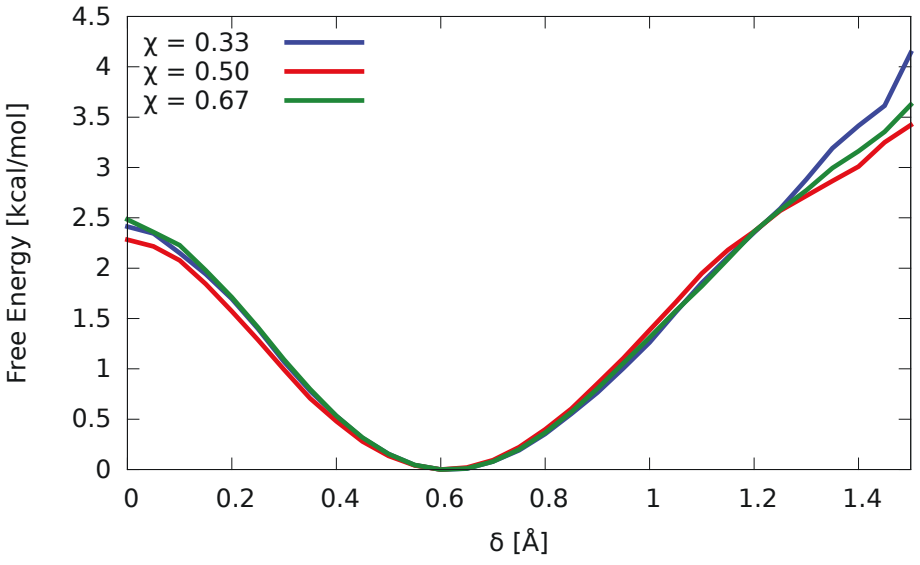

Figure 25: The PMF of proton transfer in each system.

The PMF was calculated using equations 3 and 4 where δ is the difference in the radius of the donor and the radius of the acceptor. This distance determines which species the proton is bound to and can be used to determine when the proton breaks away to bind to the acceptor.

$$\delta = |r_{N_D H^+} - r_{N_A H^+}| \tag{3}$$

The free energy can be calculated using Eq. 4 and the probability of δ (P(δ)), which is the probability that the proton will be, within the constrained radius of <2.5 Å, where a nitrogen atom exists on a Im^0 species with Eq. 3. For all mole fractions of imidazole, the energy barrier was around 2.5 kcal/mol and the concentration of imidazole did not significantly change the barrier height. Specifically, $\chi = 0.33$ had an barrier height of 2.42 kcal/mol, $\chi = 0.50$ has an activation energy of 2.28, and $\chi = 0.67$ has an activation energy of 2.48 kcal/mol.

$$\Delta F = -k_{\mathrm{B}} T \times \log\left(P(\delta)\right) \tag{4}$$

The correlation function was used to determine the timescale of proton hops using Eq. 5 and fit exponentially using Eq. 6 into a decay function. h(t) equals 1 whenever a charge belongs to the species it originated on and 0 when it hops to a new species. The results were averaged over all 16 cations in each simulation to determine the effect of added imidazole has on the timescale of proton hops.

$$c(t) = \frac{\langle h(t)h(0)\rangle}{\langle h\rangle} \tag{5}$$

In order to create the decay function, Eq. 6 was used to apply a triexponential fit where three different timescales were calculated. Since rattling events occur where a proton transfers from one species to another and then quickly back, full transfer was defined as the proton spending more than 500 fs on the species it transferred to. Such rattling events were filtered out of the calculation for the lines to be fit and the calculation was normalized so $a + b + c = 1$.

$$y = a\mathrm{e}^{-t/\tau_1} + b\mathrm{e}^{-t/\tau_2} + c\mathrm{e}^{-t/\tau_3} \quad (6)$$

Each τ in Eq. 6 calculates a different timescale of charge transfer. The order of timescales found in τ_1 were <0.1 ps while τ_2 found slightly longer timescales of 1-2 ps. Finally, τ_3 hundreds or thousands of ps. The results along with the fits used are depicted in Table 4. $\chi = 0.33$ has a considerably slower time constant for τ_3 than the systems with more imidazole due to the system having fewer and shorter wires form as was depicted in Fig. 22. The slowest timescale in all systems can be attributed to molecular reorientation which attributes to the much longer time constraint for the smallest system as reorientation into a favorable wire formation would take longer and sequential hopping is limited. The longest timescales of the other two systems, $\chi = 0.50$ and $\chi = 0.67$, were compared to previous theoretical results[8] which used a biexponential fit and depicted timescales smaller by an order of magnitude where the slowest timescale of proton transfer was 25.6 ps. The shorter timescales were found to be similar to the proposed timescale in water[25] and the longer timescales were similar to the time it takes for molecular orientation to occur to create new wires. As our results align with other

theorized values which were all directly calculated, the triexponential fit in Eq. 6 likely gives accurate timescales.

Table 4: Fitting parameters for triexponential decay functions to the charge correlation.

Mole Fraction of Imidazole	a	τ_1 (ps)	b	τ_2 (ps)	c	τ_3 (ps)	τ_{fit} (ps)
0.33	0.010	0.063	0.025	0.81	0.965	2474	2387
0.50	0.030	0.082	0.074	1.72	0.896	772	692
0.67	0.041	0.121	0.054	1.66	0.905	427	387

Greater decay in Fig. 26 depicts faster proton transfer. The smallest system shows little decay as there is not as much opportunity for proton transfer with the small amount of solvent added. As concentration of imidazole increases, greater decay is depicted as most of the protons are able to transfer quickly when more imidazole is available to form wires. Therefore, a greater percentage of protons will transfer on small timescales and the graph decays.

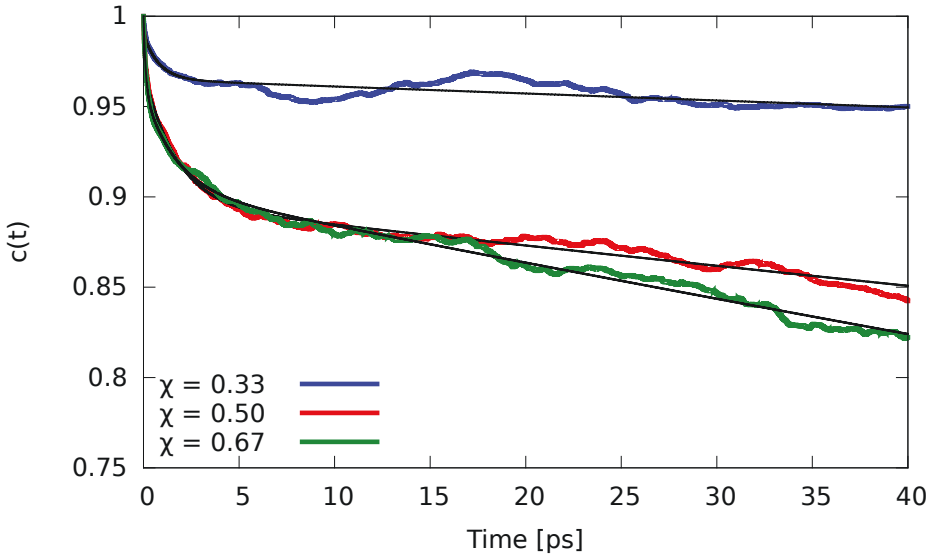

Figure 26: The unfiltered correlation function of proton transfer with the triexponential fits.

Similarly, the hydrogen bond correlation function was also determined using Eq. 5 and Eq. 6 again. Additional criteria in defining hydrogen bonds were added so that the distance between species was constrained to 2.5 Å and the bond angle between the nitrogen, excess proton attached to the nitrogen, and the next species was less than 22.5°. Since hydrogen bonding is essential to proton transfer, the hydrogen bond was not considered to be broken in the event of proton transfer and the proton was considered to be shared by the two species so long as the length and angle requirements for a hydrogen bond remained. The rate of decay in Fig. 27 was much slower than in Fig. 26 due to the strong affinity of the cation to Im^0 as opposed to $TFSI^-$. Because Im^0 species form strong, long-lasting hydrogen bonds, the timescale of hydrogen bonds will increase as imidazole is added. When more imidazole becomes available to become part of the network, more instances of hydrogen bonding occur and due to the stability of the hydrogen bonds, they will occur for a long timescale.

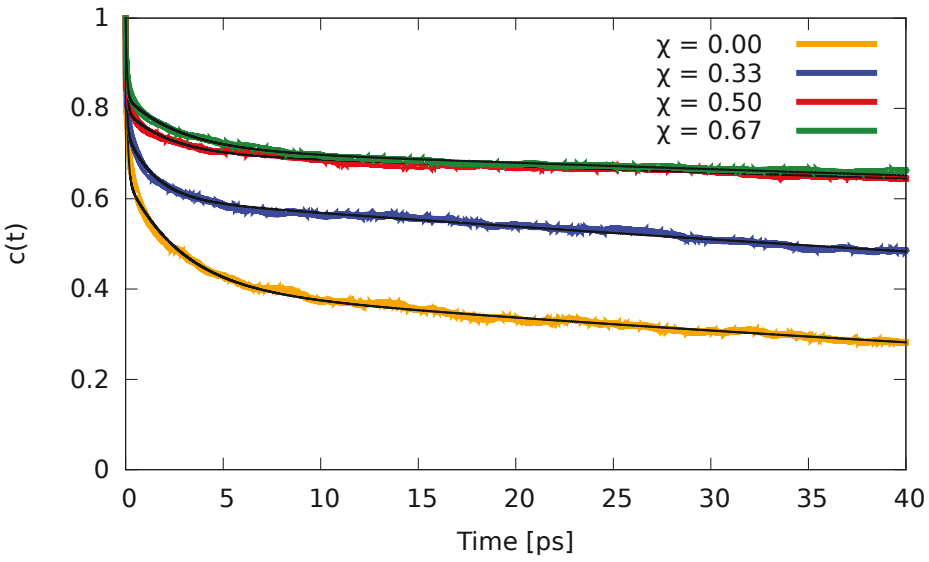

Figure 27: Hydrogen-bond correlation function with the calculated triexponential fits.

4. HIm^+ Systems

HIm^+ systems were run similarly to C_2HIm^+: $TFSI^-$ was used as the anion with systems doped with different ratios of imidazole to HTFSI (2:1 and 3:1). No 1:1 system was tested because the results of the C_2HIm^+ system showed no proton transfer in the pure IL. Instead of $C2HIm^+$, this simulation used unsubstituted imidazolium (Im^+) as the cation and the temperature was varied to determine the effect of temperature on proton transport. Previous experimental work[12] has shown that proton transport changes in regards to temperature as the Grotthuss mechanism requires a network to form and this network can be disrupted by temperature. At the same time, the formation of the network requires enough energy for imidazole to reorient appropriately. Therefore, identical systems were simulated at 303 K, 343 K, and 383 K. The simplicity of this system, made my mixing HTFSI and a surplus of imidazole together, makes it ideal to study temperature dependence and proton hopping.

The RDFs of the excess proton to the anion show minimal interaction. Fluorine forms no solvation shell around the cation. Oxygen and nitrogen minimally solvate the excess proton at a hydrogen bond distance of 1.90 Å. The solvation structure of HIm^+ is dominated by Im^0 which indicates strong interaction between imidazole species and the excess proton.

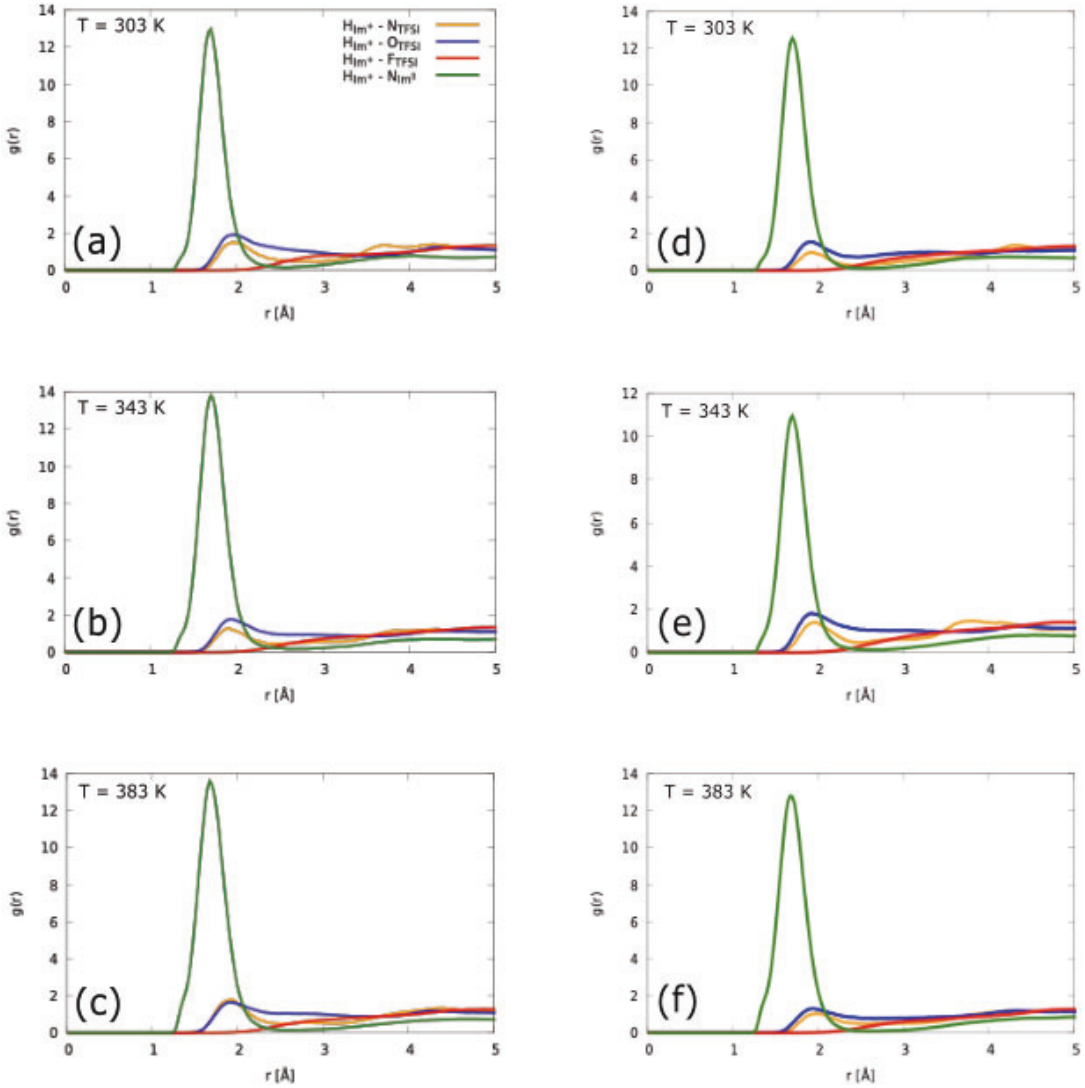

Figure 28: RDF of H_{Im}^+ to other Im^0 species and the oxygen, nitrogen, and fluorine atoms on TFSI for each temperature for the 2:1 system (a, b, c) and the 3:1 system (d, e, f).

The species were defined differently for the HIm^+ systems than the C_2HIm^+ since imidazole becomes identical to the cation once a proton transfers in the HIm^+ system. Although the positive charge traveled with the proton in the C_2HIm^+ system, the original cation (C_2HIm^+) has an ethyl group attached and can never be in the middle of a wire. For this reason, C_2HIm^+ was defined as Im^+ and added imidazole species were defined as Im^0, whether or not they had accepted an excess proton from the cation. This was changed when calculating the RDF of the HIm^+ systems because the cation (imidazolium) is a regular imidazole ring with an excess proton. That is, when the added imidazole species accepted the proton, they became the cation and it was defined as such in the calculations. This is due to the fact that imidazolium does not necessarily cap the imidazole wire as C_2HIm^+ would. Unsubstituted imidazolium may have wires of hydrogen bonded imidazole extending out from both sides and the excess proton can hop in either direction. Once this happens, the original cation becomes a regular member of an imidazole wire, ready to accept the excess proton. Therefore, in these RDFs, HIm^+ shows the solvation structure the acidic proton attached to any given (Im^+) and Im^0 represents any imidazole without an excess proton attached.

There is no ownership peak at 1 Å as the identity of the cation changes as soon as the proton transfers to another imidazole. The Im^0 the proton transfers to instantly becomes defined as the new Im^+, and therefore the RDF never shows Im^0 owning H_{Im}^+.

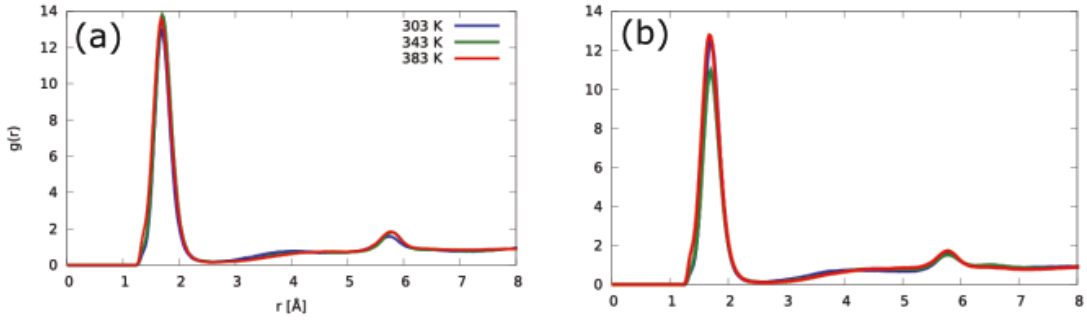

Figure 29: RDF of H_{Im}^+ to Im^0 species in the 2:1 system (a) and the 3:1 system (b).

Due to how the cation was identified in the calculations, an absence of an ownership peak does not indicate the proton never transferred to a new imidazole. Greater hopping numbers can be seen in Table 5 with both an increase in imidazole and an increase in temperature, indicating that imidazole concentration influenced hopping. The solvation of the proton by the original Im^+ can be seen in the RDF as the small density beginning at 1.20 Å and appears on the graph. The structure of the original Im^+ is present as soon as the proton transfers to Im^0 and the definition of the cation changes. Therefore, the RDFs indicate proton transfer among imidazole species. The peak continues to form the

Table 5: The total proton hops in each system.

Temperature	Hops/ps 2:1	Hops/ps 3:1
303 K	660	660
343 K	887	1102
383 K	1344	2665

primary peak in the graph which centers at 1.70 Å and shows imidazole closely solvating the proton.

The various temperatures had no bearing on the solvation structure around H_{Im}^{+}. A hydrogen bond peak can be seen for all systems indicating Im^{0} directly beside H_{Im}^{+} and interacting with it. Additionally, imidazole continues to form a strong solvation structure at 5.78 Å which indicates another imidazole species next to the imidazole directly solvating H_{Im}^{+} and forming a structured wire in all systems.

Temperature makes little difference on the coordination numbers, although slightly less coordination around H_{Im}^{+} can be seen at 303 K. As with the RDFs, there is no coordination at 1 Å due to the changed identity of the cation as soon as the proton hops. However, strong hydrogen bonding can be seen at 2.08 Å indicating Im^{0} interacting with H_{Im}^{+} and positioned to accept the proton.

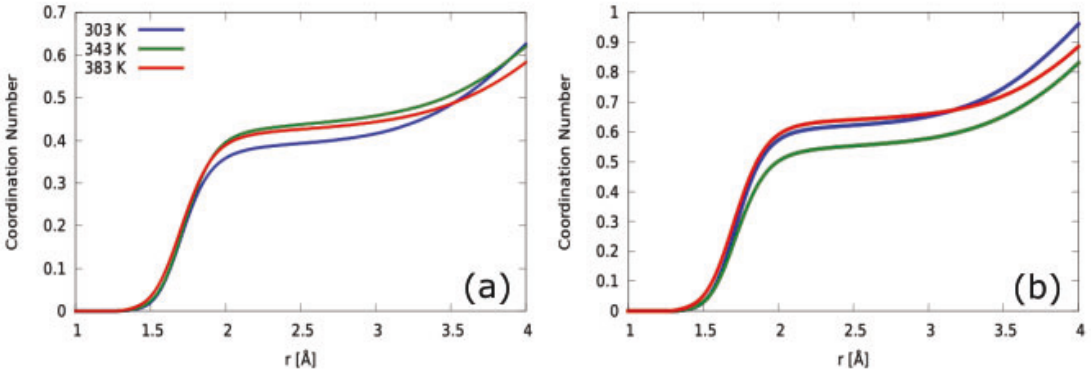

Figure 30: The coordination number of H_{im}^{+} to Im^{0} for the 2:1 system (a) and the 3:1 system (b).

The diffusion of each species is summarized in Table 6. Proton diffusion was not greatly influenced by temperature, but increasing the concentration of neutral species more than doubled the proton coefficient of self-diffusion. However, the diffusion of the ions themselves increased with temperature, but were not notably influenced by the concentration of neutral imidazole. The ratio of the diffusion of H^+ to the diffusion of imidazole decreased with temperature, following a trend also seen in previous experimental results.[12]

Table 6: The diffusion of each species in the HIm^+ systems. [a]D_{Im} includes both Im^+ and Im^0 rings.

Im^0:HTFSI	Temperature	D_{H^+} $[10^3\ Å^2/ps]$	D_{Im} $[10^3\ Å^2/ps]^a$	D_{TFSI^-} $[10^3 Å^2/ps]$	D_{H^+} $/D_{\mathrm{Im}}$
2:1	303	9.45	4.52	1.78	2.09
	343	9.67	4.70	1.81	2.06
	383	9.83	6.61	3.57	1.60
3:1	303	22.1	3.98	1.85	5.55
	343	21.8	5.10	2.01	4.27
	383	27.1	7.14	4.81	3.80

Temperature has little effect on the PMF, as calculated from Eq. 3 and Eq. 4. The energy barrier 2.32 kcal/mol for 303 K, 2.42 kcal/mol for 343 K, and 383 K is 2.35 kcal/mol.

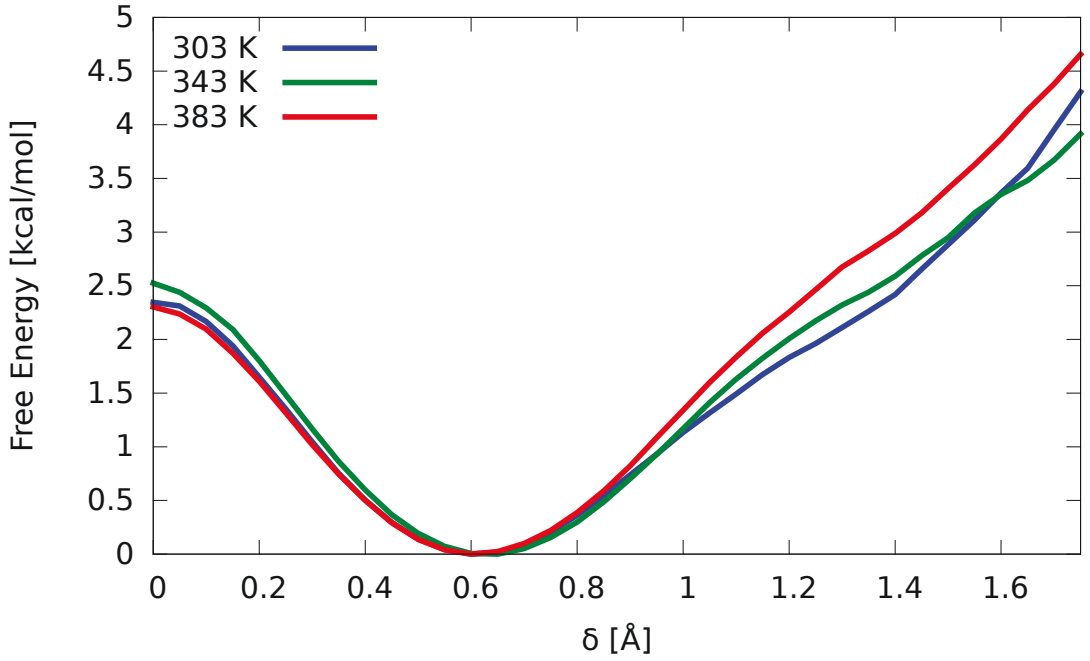

Figure 31: The potential mean force for the 2:1 system.

The correlation function in Fig. 32 shows a much greater rate of decay in the 3:1 system than 2:1. Moreover, temperature leads to greater decay as it is increased due to the increased energy allotted to allow the proton to overcome the energy barrier. Fig. 31(b) shows that the 3:1 system at 383 K showed the fastest proton transfer as the greater amount of imidazole allowed for more wire formation and the increased temperature allowed for the quick breakage and reformation of bonds.

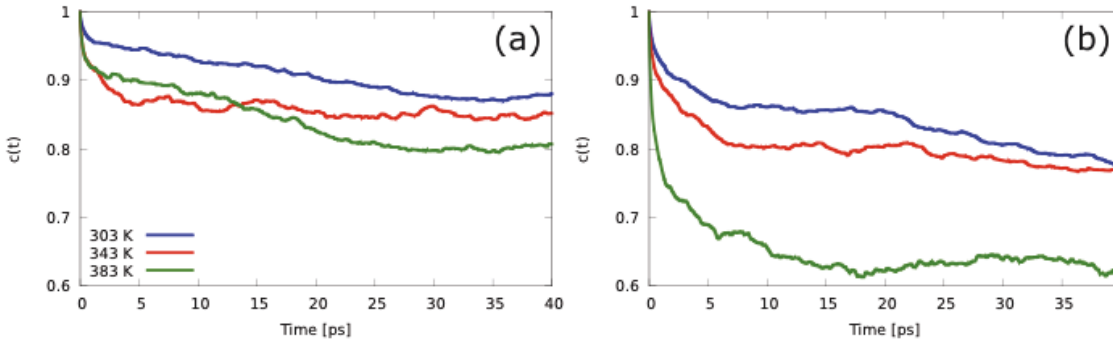

Figure 32: The proton correlation function of 2:1 (a) and 3:1 (b).

5. Solvate Systems

SILs are another area of interest to research proton transport as proton hopping has been shown to occur. A simple system containing 12 ion pairs of hydronium (H_3O^+) solvated by 18C6 with and solvent additions were created and the simulations were all run at 348 K. The solvent, water, was added as 6 species ($\chi = 0.33$), 12 species ($\chi = 0.50$), 24 species ($\chi = 0.67$), and one system was created with only the pure IL. Identical simulations were created with two different anions: HTFSI, a superacid, and acetic acid, a much weaker acid. The difference in solvation structure and mechanism of proton transport was studied in the two systems.

5.1 $TFSI^-$

The system with $TFSI^-$ was analyzed first. The RDF of H_3O^+ to the system was calculated in order to determine the solvation around the cation. As seen in Fig. 33 the

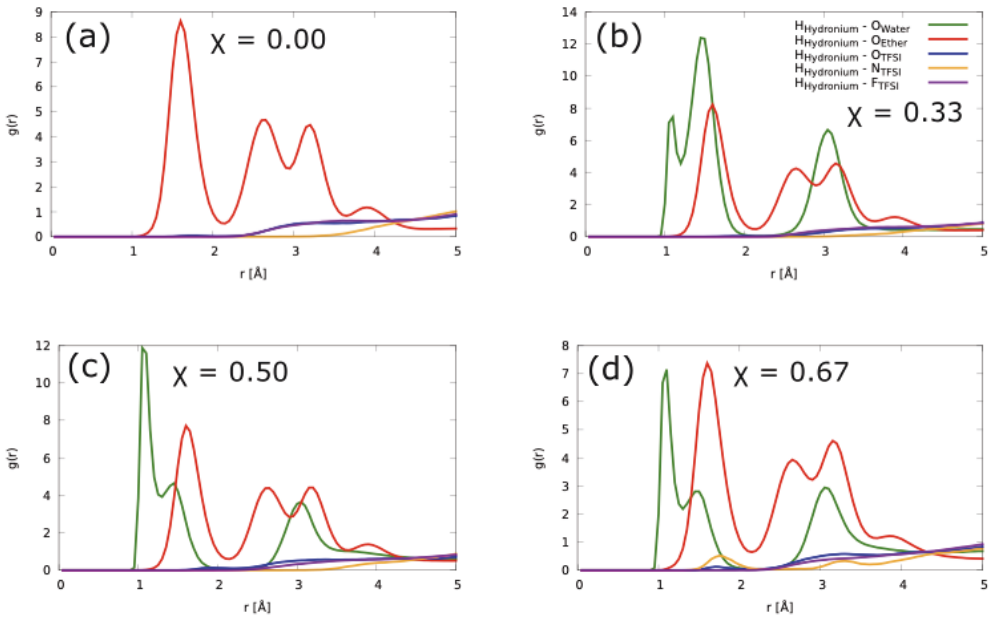

Figure 33: The solvation structure around hydronium in each system.

solvation structure of the pure system is dominated by ether, however when water was added, water more strongly solvated H_3O^+ than 18C6. Peaks at various distances indicates a structured wire formation of the water species. This pattern is similar to the pattern of 18C6 around H_3O^+, but the multiple peaks are due to multiple oxygen species in the crown ether. The solvation structure of $TFSI^-$ around H_3O^+ is virtually nonexistent compared with the structure of the solvent and the ether. Nitrogen weakly solvates H_3O^+ at 1.75 Å and at 3.30 Å, but there is otherwise negligible interaction between the ion pairs.

Because water is the conjugate base of hydronium, the RDFs were determined without differentiating between cations as the excess proton transferred from water-to-water. Therefore, the solvation structure of water around H_3O^+ of all three systems shows a peak centered at 1.05 Å, indicating the cation's ownership of the proton. A second peak centered at 1.45 Å indicates the presence of a bridging water molecule where the proton is transferred. Another peak centered at 3.05 Å indicates the formation of a water wire

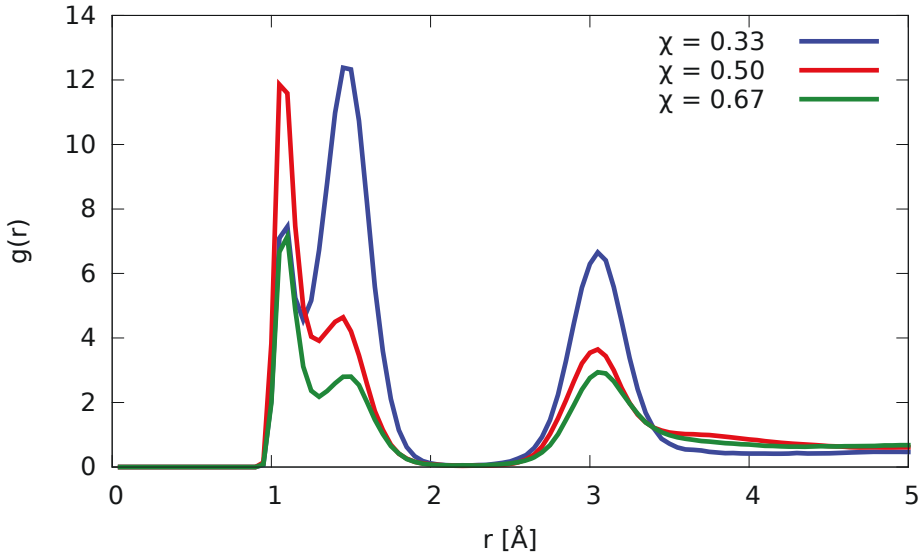

Figure 34: The RDF of hydronium to water.

beyond the ether. Therefore, water was able to enter the solvation shell created by 18C6 and can potentially transport a proton outside the solvation shell and across a system via the Grotthuss mechanism due to the bridging water.

The coordination number in Fig. 35 shows a plateau at 1.15 Å indicates that slightly less than 20% of H_3O^+ species are solvated by water and that all three systems follow the same trend, regardless of how much water is added. This indicates that H_3O^+ transfers the excess proton to a bridging water molecule. Although this is the obvious plateau, a small plateau can also be seen at 1.10 Å which represents the proton bound to the original cation.

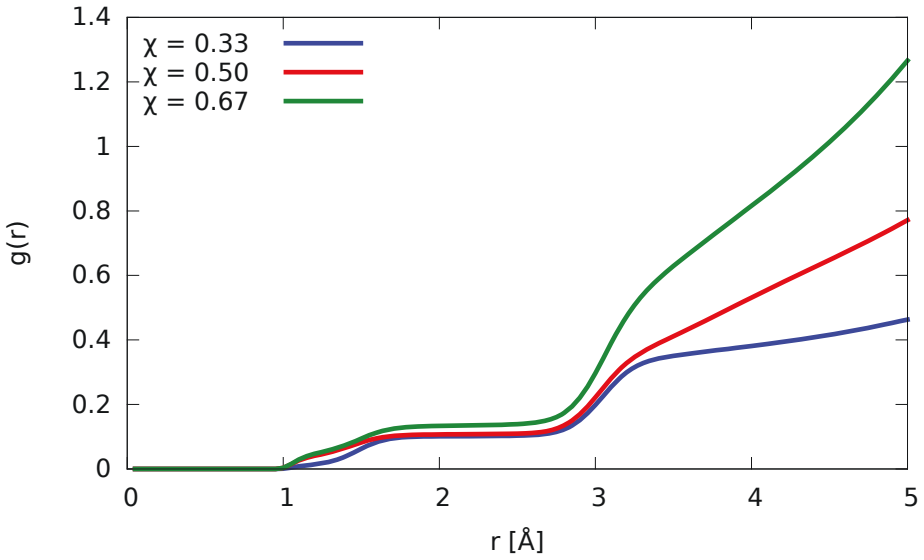

Figure 35: The coordination number of hydronium to water.

Therefore, the excess proton is able to transfer from the crown ether shell via a bridging water. As shown in Fig. 36 a water molecule inserted into the solvation shell of 18C6 and interacted with hydronium as well as 18C6. From there, hydronium is able to pass the proton to water which may in turn pass to a proton to water molecules outside the solvation shell and across the system.

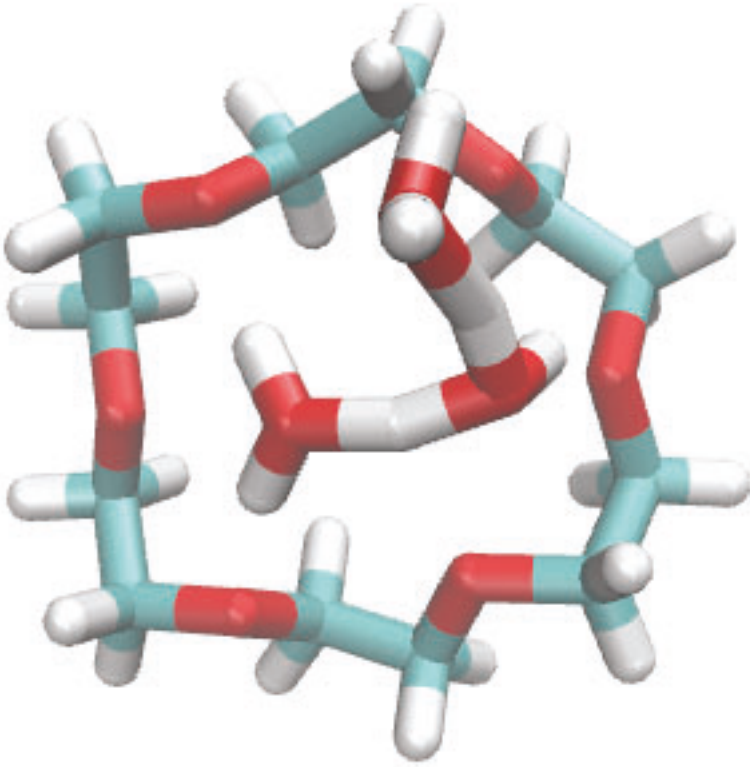

Figure 36: A hydronium ion solvated by 18-crown-6-ether forming a hydrogen bond network with two water species.

An analysis of overall hopping trends showed that hopping increased with the addition of water as per Table 7, but hopping was not limited to systems containing water. The pure IL system showed an average of 26.48 hops/ps, indicating the proton transfers to 18C6 as the proton is unable to transfer to $TFSI^-$. This can also be seen in Fig. 32 where

a peak centered at 1.60 Å indicates ether's ownership of the proton. Therefore, it can be determined that the instances of hops in the pure system are rattling occurances where the proton hops back and forth between the H_3O^+ and 18-crown-6-ether. The charge stays localized on the cation-ether complex and diffusion does not increase.

Table 7: Total hops in the TFSI- solvate system.

Mole Fraction of Water	Hops/ps
0.00	26.48
0.33	61.36
0.50	73.37
0.67	99.07

The proton hops began to increase with increasing additions of solvent (see Table 7) because then the water was able to participate in the Grotthuss mechanism by accepting a proton from hydronium. Due to water's size, the species was able to enter the ether solvation ring and accept the proton instead of 18C6 due to its high affinity for the proton compared to 18C6. Another water molecule is also able to insert itself into the ring to facilitate in the transport of the proton outside the complex as shown in Fig. 36. Once outside the complex, the charge is able to transport across the system using the network of water species as shown in Fig. 37 where the bridging water can be seen creating a connection between H_3O^+ and a wire of water outside the complex. Strong hydrogen bonds are present between the water molecules and H_3O^+ to facilitate proton transport, but hydrogen bonds are also present between water and 18C6. Since the proton's affinity to water is greater than the affinity to 18C6, the proton continues to hop along the water network to diffuse the charge through the system. The bridging water's

hydrogen bond with 18C6 anchors it to the solvation shell while the other hydrogen is able to interact with the water molecules outside of the solvation shell.

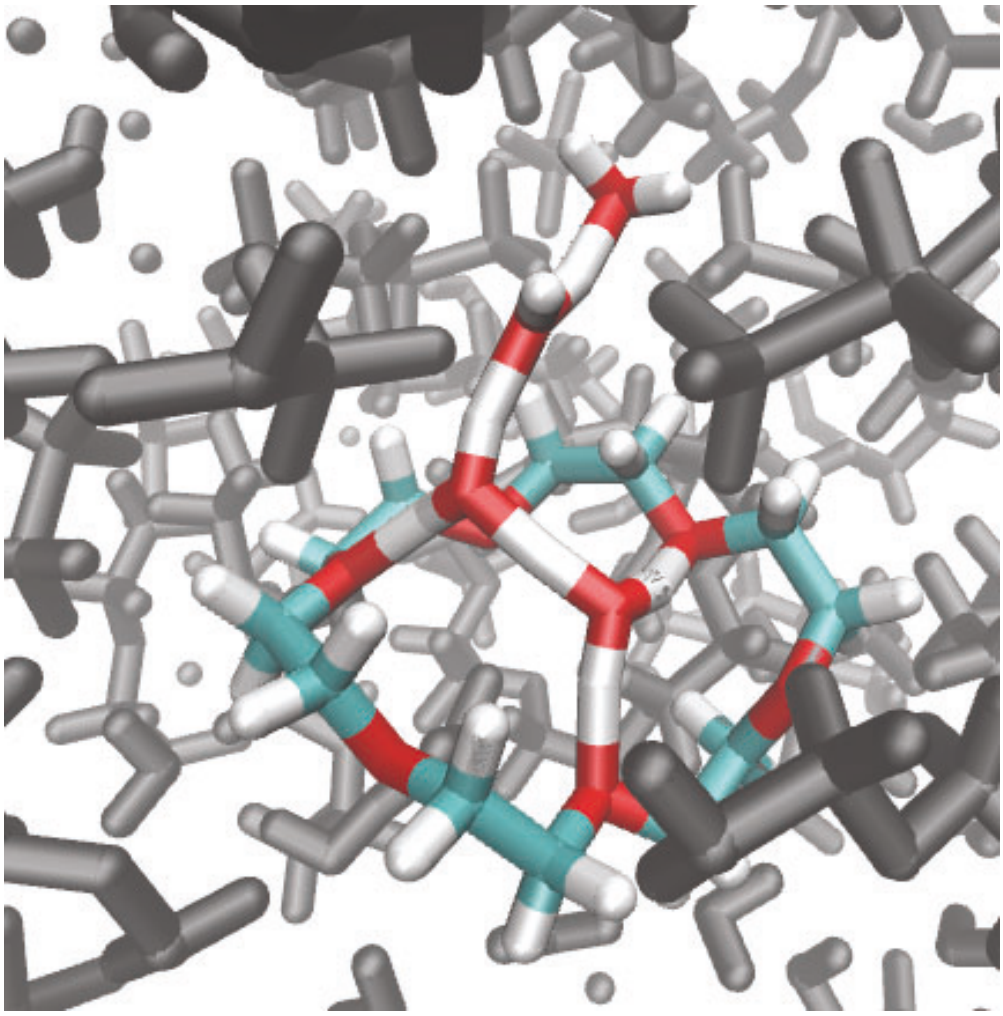

Figure 37: Wire formation of water species.

5.2 Acetate

The RDF of water to the system in Fig. 38 shows that acetate dominates the solvation structure with a peak centered at 1.05 Å, indicating ownership of the proton. In comparison, water shows a weak peak with no ownership.

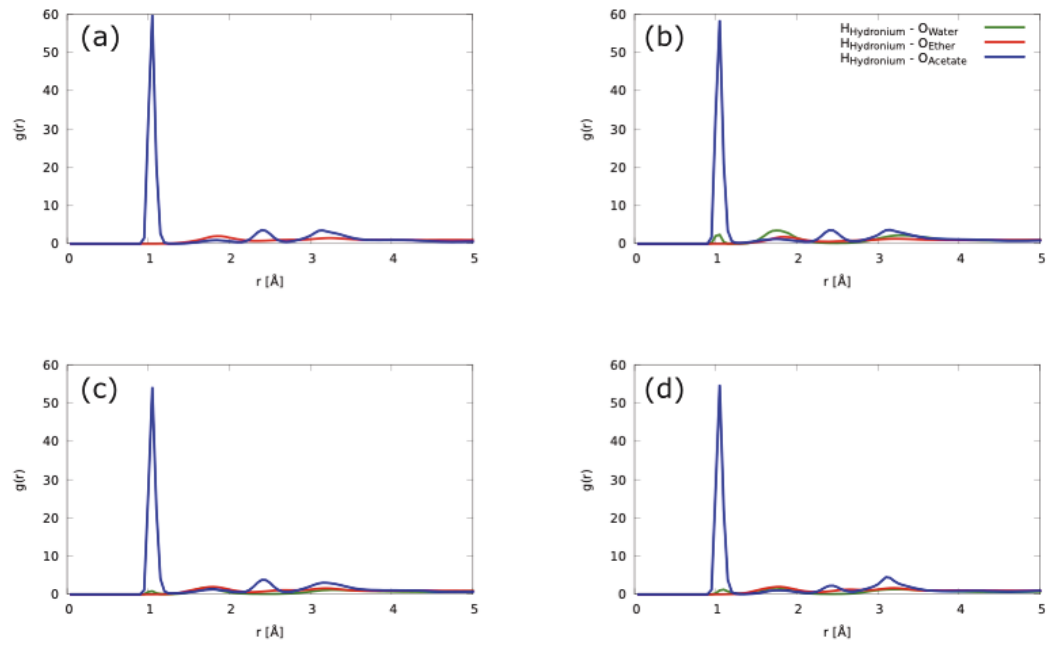

Figure 38: RDFs of H_3O^+ to the system for the pure system (a), $\chi = 0.33$ (b), $\chi = 0.50$ (c), and $\chi = 0.67$ (d).

The solvation structure of H_3O^+ did not vary much between additions of solvent. A second solvation peak can be seen at 2.40 Å and a third at 3.1 Å which indicates other acetate species hydrogen-bonding with the cation.

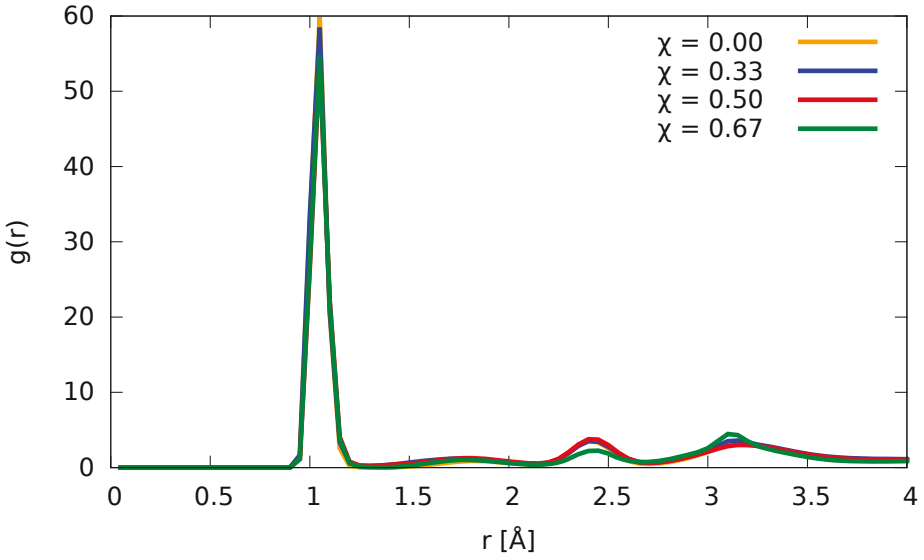

Figure 39: The RDF of hydronium to acetate.

The coordination number in Fig. 40 shows that around 82% of protons transfer to acetate and around 10% are solvated by acetate through hydrogen-bonding. The mole fraction of water makes no difference in the solvation structure as acetate dominates the solvation of the proton.

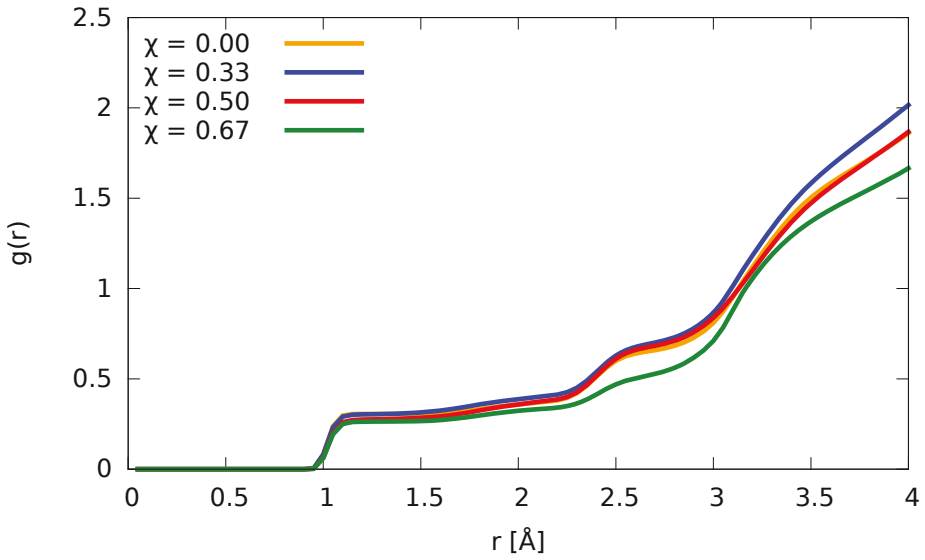

Figure 40: The coordination number of hydronium to acetate.

Proton hopping also increased with mole fraction of water in the acetate system (Table 8). However, there were generally fewer hops overall. Acetate blocks hopping events by accepting and not donating the proton as it has not been shown to use the Grotthuss mechanism. Acetate's conjugate acid has a relatively high $\mathrm{p}K_{\mathrm{a}}$ (4.8 in water), allowing it to more readily accept a proton than water. In addition, acetate is a small molecule which can position itself in the crown ether and accept the proton like water. Because acetate has a higher affinity for the proton than water, it accepts the proton.

Table 8: Average number of total hops in the acetate system.

Mole Fraction of Water	Hops/ps
0.00	4.36
0.33	10.03
0.50	16.23
0.67	19.51

6. Conclusion

Proton transport studied in three different simple sets of simulations showed that the amount of solvent added directly affects proton transport. In Chapter 3, it was found that greater concentrations of imidazole added to [C_2HIm^+][$TFSI^-$] gave way to more overall proton hops and higher diffusion constants. Similarly, the SIL with $TFSI^-$ showed increased proton hops with additions of water. The addition of amphoteric solvents to these ILs allowed for the formation of hydrogen bond networks which were then used to transport the charge across the system. Greater amounts of solvent allowed for more instances of network formation as well as for longer networks to form leading to greater diffusion of the proton.

This was facilitated by the presence of HTFSI, a superacid which supplied protons to the system and subsequently acted as the anion for the imidazolium species. Due to the low $\mathrm{p}K_\mathrm{a}$ of the superacid, $TFSI^-$ did not interfere with proton transport as it was unable to accept a proton and only weakly hydrogen bonded with the acidic proton. Simulations run with $TFSI^-$ were compared to identical simulations which used acetate as the anion instead and showed that acetate dominated solvation of the acidic proton in every instance. The C_2HIm^+ simulations with acetate were not continued past equilibration due to the decrease in hopping that occurred when solvent was added as the addition of Im^0 interfered with acetate's ability to accept the proton. The SIL, on the other hand, still

displayed increasing hops with additions of solvent, but acetate dominated the solvation structure of the proton.

The effect of temperature was also determined in a very simple [Im^+][$TFSI^-$] system in Chapter 4, although a temperature range of 80 K did not show a great difference in the energy barrier of proton transfer. However, the correlation function determined that proton transfer occurred faster with increased concentrations of imidazole and increased temperature. Temperature also had an effect on the diffusion of the parent ions through the system, but not the diffusion of the charge. The ratio of proton diffusion over ion diffusion therefore decreased as temperature increased, following the same trend as seen in previous experimental work.

The overarching conclusions of these three studies determines that temperature and ionicity are vital to the success of the Grotthus mechanism to transport protons.the Grotthuss mechanism is possible when a highly acidic anion is used and neutral species come from added solvent with amphoteric properties. As such, these systems and modifications thereof can potentially be used to increase the efficiency of fuel cells for the production of greener energy.

References

(1) Hallett, J. P.; Welton, T. Room-Temperature Ionic Liquids: Solvents for Synthesis and Catalysis. 2. *Chemical Reviews* **2011**, *111* (5), 3508-3576. DOI: 10.1021/cr1003248.

(2) Ruckart, K. N.; O'brien, R. A.; Woodard, S. M.; West, K. N.; Glover, T. G. Porous Solids Impregnated with Task-Specific Ionic Liquids as Composite Sorbents. *Journal of Physical Chemistry C* **2015**, *119*, 20681-20697.

(3) Hoogerstraete, T. V.; Onghena, B.; Binnemans, K. Homogeneous Liquid-Liquid Extraction of Metal Ions with a Functionalized Ionic Liquid. *J Phys Chem Lett* **2013**, *4* (10), 1659-1663. DOI: 10.1021/jz4005366 From NLM.

(4) Yaghini, N.; Nordstierna, L.; Martinelli, A. Effect of water on the transport properties of protic and aprotic imidazolium ionic liquids - an analysis of self-diffusivity, conductivity, and proton exchange mechanism. *Phys Chem Chem Phys* **2014**, *16* (20), 9266-9275. DOI: 10.1039/c4cp00527a From NLM.

(5) Yaghini, N.; Gómez-González, V.; Varela, L. M.; Martinelli, A. Structural origin of proton mobility in a protic ionic liquid/imidazole mixture: insights from computational and experimental results. *Phys Chem Chem Phys* **2016**, *18* (33), 23195-23206. DOI: 10.1039/c6cp03058k From NLM.

(6) Grotthuss, C. J. T. v. Sur la décomposition de l'eau et des corps q'uelle tient en dissolution à l'aide de l'électricité galvanique. *Annales de Chimie* **1806**, *LVIII* 54-74.

(7) Atkins, P. W.; Julio, D. P.; James, K. *Physical chemistry*; 2018.

(8) Long, Z.; Atsango, A. O.; Napoli, J. A.; Markland, T. E.; Tuckerman, M. E. Elucidating the Proton Transport Pathways in Liquid Imidazole with First-Principles Molecular Dynamics. *J Phys Chem Lett* **2020**, *11* (15), 6156-6163. DOI: 10.1021/acs.jpclett.0c01744 From NLM.

(9) Hasani, M.; Varela, L. M.; Martinelli, A. Short-Range Order and Transport Properties in Mixtures of the Protic Ionic Liquid [C2HIm][TFSI] with Water or Imidazole. *The Journal of Physical Chemistry B* **2020**, *124* (9), 1767-1777. DOI: 10.1021/acs.jpcb.9b10454.

(10) Feng, Q.; Yuan, X. Z.; Liu, G.; Wei, B.; Zhang, Z.; Li, H.; Wang, H. A review of proton exchange membrane water electrolysis on degradation mechanisms and mitigation strategies. *Journal of Power Sources* **2017**, *366*, 33-55. DOI: https://doi.org/10.1016/j.jpowsour.2017.09.006.

(11) Zięba, S.; Dubis, A.; Ławniczak, P.; Gzella, A.; Pogorzelec-Glaser, K.; Łapiński, A. Effect of counter ions on physical properties of imidazole-based proton conductors. *Electrochimica Acta* **2019**, *306*, 575-589. DOI: https://doi.org/10.1016/j.electacta.2019.03.125.

(12) Hoarfrost, M. L.; Tyagi, M.; Segalman, R. A.; Reimer, J. A. Proton Hopping and Long-Range Transport in the Protic Ionic Liquid [Im][TFSI], Probed by Pulsed-Field Gradient NMR and Quasi-Elastic Neutron Scattering. *The Journal of Physical Chemistry B* **2012**, *116* (28), 8201-8209. DOI: 10.1021/jp3044237.

(13) Kitada, A.; Kintsu, K.; Takeoka, S.; Fukami, K.; Saimura, M.; Nagata, T.; Katahira, M.; Murase, K. A Hydronium Solvate Ionic Liquid: Ligand Exchange Conduction Driven by Labile Solvation. *Journal of The Electrochemical Society* **2018**, *165*.

(14) Molina, P.; Tárraga, A.; Otón, F. Imidazole derivatives: a comprehensive survey of their recognition properties. *Org Biomol Chem* **2012**, *10* (9), 1711-1724. DOI: 10.1039/c2ob06808g From NLM.

(15) Salahuddin; Shaharyar, M.; Mazumder, A. Benzimidazoles: A biologically active compounds. *Arabian Journal of Chemistry* **2017**, *10*, S157-S173. DOI: https://doi.org/10.1016/j.arabjc.2012.07.017.

(16) Brehm, M.; Weber, H.; Pensado, A. S.; Stark, A.; Kirchner, B. Proton transfer and polarity changes in ionic liquid-water mixtures: a perspective on hydrogen bonds from ab initio molecular dynamics at the example of 1-ethyl-3-methylimidazolium acetate-water mixtures--part 1. *Phys Chem Chem Phys* **2012**, *14* (15), 5030-5044. DOI: 10.1039/c2cp23983c From NLM.

(17) Rey-Castro, C.; Tormo, A. L.; Vega, L. F. Effect of the flexibility and the anion in the structural and transport properties of ethyl-methyl-imidazolium ionic liquids. *Fluid Phase Equilibria* **2007**, *256* (1), 62-69. DOI: https://doi.org/10.1016/j.fluid.2006.09.027.

(18) Eyckens, D. J.; Henderson, L. C. A Review of Solvate Ionic Liquids: Physical Parameters and Synthetic Applications. *Front Chem* **2019**, *7*, 263. DOI: 10.3389/fchem.2019.00263 From NLM.

(19) Tamura, T.; Yoshida, K.; Hachida, T.; Tsuchiya, M.; Nakamura, M.; Kazue, Y.; Tachikawa, N.; Dokko, K.; Watanabe, M. Physicochemical Properties of Glyme–Li Salt Complexes as a New Family of Room-temperature Ionic Liquids. *Chemistry Letters - CHEM LETT* **2010**, *39*, 753-755. DOI: 10.1246/cl.2010.753.

(20) Martínez, L.; Andrade, R.; Birgin, E. G.; Martínez, J. M. PACKMOL: A package for building initial configurations for molecular dynamics simulations. *Journal of Computational Chemistry* **2009**, *30* (13), 2157-2164, https://doi.org/10.1002/jcc.21224. DOI: https://doi.org/10.1002/jcc.21224 (acccessed 2022/06/02).

(21) Canongia Lopes, J. N.; Pádua, A. A. H. CL&P: A generic and systematic force field for ionic liquids modeling. *Theoretical Chemistry Accounts* **2012**, *131* (3), 1129. DOI: 10.1007/s00214-012-1129-7.

(22) Jorgensen, W. L.; Maxwell, D. S.; Tirado-Rives, J. Development and Testing of the OPLS All-Atom Force Field on Conformational Energetics and Properties of Organic Liquids. *Journal of the American Chemical Society* **1996**, *118* (45), 11225-11236. DOI: 10.1021/ja9621760.

(23) Wu, Y.; Tepper, H. L.; Voth, G. A. Flexible simple point-charge water model with improved liquid-state properties. *J Chem Phys* **2006**, *124* (2), 024503. DOI: 10.1063/1.2136877 From NLM.

(24) Kühne, T. D.; Iannuzzi, M.; Del Ben, M.; Rybkin, V. V.; Seewald, P.; Stein, F.; Laino, T.; Khaliullin, R. Z.; Schütt, O.; Schiffmann, F.; et al. CP2K: An electronic structure and molecular dynamics software package - Quickstep: Efficient and accurate electronic structure calculations. *The Journal of Chemical Physics* **2020**, *152* (19), 194103. DOI: 10.1063/5.0007045 (acccessed 2022/06/02).

(25) Arntsen, C.; Chen, C.; Calio, P. B.; Li, C.; Voth, G. A. The hopping mechanism of the hydrated excess proton and its contribution to proton diffusion in water. *The Journal of*

Chemical Physics **2021**, *154* (19), 194506. DOI: 10.1063/5.0040758 (acccessed 2022/05/21).